Title

Identification of a novel arthritis-associated osteoclast precursor macrophage regulated by FoxM1

Authors

Tetsuo Hasegawa[1,2], Junichi Kikuta[1,3], Takao Sudo[1], Yoshinobu Matsuura[1], Takahiro Matsui[1], Szandor Simmons[1], Kosuke Ebina[4], Makoto Hirao[4], Daisuke Okuzaki[5], Yuichi Yoshida[6], Atsushi Hirao[7], Vladimir V. Kalinichenko[8], Kunihiro Yamaoka[2], Tsutomu Takeuchi[2], Masaru Ishii[1,3]*

Affiliations

[1]Department of Immunology and Cell Biology, Graduate School of Medicine and Frontier Biosciences, Osaka University, Osaka, Japan

[2]Division of Rheumatology, Department of Internal Medicine, Keio University School of Medicine, Tokyo, Japan

[3]WPI-Immunology Frontier Research Center, Osaka University, Osaka, Japan

[4]Department of Orthopaedic Surgery, Osaka University, Osaka, Japan

[5]Genome Information Research Center, Research Institute for Microbial Diseases, Osaka University, Osaka, Japan

[6]Department of Gastroenterology and Hepatology, Osaka University, Osaka, Japan

[7]Division of Molecular Genetics, Cancer Research Institute, WPI Nano Life Science Institute (WPI-Nano LSI), Kanazawa University, Kanazawa, Japan

[8]Center for Lung Regenerative Medicine, Division of Pulmonary Biology, Cincinnati Children's Hospital Medical Center, Cincinnati, USA

Correspondence to

Masaru Ishii, Department of Immunology and Cell Biology, Osaka University Graduate School of Medicine and Frontier Biosciences, 2-2 Yamada-oka, Suita, Osaka 565-0871, Japan

Email: mishii@icb.med.osaka-u.ac.jp

Abstract

Osteoclasts have a unique bone-destroying capacity, playing key roles in steady-state bone remodelling and arthritic bone erosion. Whether these two populations of osteoclasts in different tissue settings arise from the same precursor states of monocytoid cells is presently unknown. Here, we show that osteoclasts in pannus originate exclusively from circulating bone marrow-derived cells and not from locally resident macrophages. We identify $CX_3CR1^{hi}Ly6C^{int}F4/80^{+}I\text{-}A/I\text{-}E^{+}$ macrophages (termed “arthritis-associated osteoclastogenic macrophages [AtoMs]”) as the osteoclast precursor (OP)-containing population in the inflamed synovium, comprising a subset distinct from conventional OPs in homeostatic bone remodelling. Tamoxifen-inducible FoxM1 deletion suppressed the capacity of AtoMs to differentiate into osteoclasts *in vitro* and *in vivo*. Furthermore, synovial samples from human rheumatoid arthritis (RA) patients contained $CX_3CR1^{+}HLA\text{-}DR^{hi}CD11c^{+}CD80^{-}CD86^{+}$ cells that corresponded to human AtoMs, and osteoclastogenesis was inhibited by the FoxM1 inhibitor,

thiostrepton, constituting a potential target for RA treatment.

Introduction

Macrophages comprise a variety of subsets with diverse biological activities, contributing to tissue homeostasis and a broad spectrum of pathogenesis[1–4]. In response to environmental cues, they follow distinct developmental pathways, such as differentiation into osteoclasts. Osteoclasts are myeloid lineage cells with unique bone-destroying capacity and require macrophage-colony stimulating factor (M-CSF) and receptor activator of NF-κB ligand (RANKL) for differentiation and survival[5,6]. They play a key role in maintaining skeletal homeostasis by supporting steady-state bone remodelling in the bone marrow (BM). However, in contrast to this physiological role, osteoclasts are also involved in pathological arthritic bone erosion in patients with rheumatoid arthritis (RA), which occurs where the hypertrophied synovium[7] (called “pannus”) invades the outer surface of the articular bone[6]. Previous studies have determined that the Ly6C^{hi} monocytic population in the BM contains osteoclast

precursors (OPs) in arthritic mice[8,9], and a recent study demonstrated that CX_3CR1 could be a marker for osteoclasts differentiated from BM-derived dendritic cells in inflammatory conditions[10]. Nevertheless, a precise analysis of OPs has not yet been performed in “inflamed synovium”, the actual site of bone erosion in arthritis, mainly due to technical difficulties associated with approaching and isolating tiny synovial tissues on the so-called “bare area”[11], where bone is exposed to synovium without a cartilage covering and, therefore, vulnerable to erosion. It remains unknown whether the two osteoclast populations in the BM and synovial tissue settings share similar differentiation pathways and arise from similar precursor states of monocytoid cells[12]. In addition, while it has been suggested that osteoclasts in pannus derive from blood, the empirical evidence for this relationship is lacking.

In this study, we have developed a new protocol to isolate the inflamed synovium on the bare area[11] of arthritic mice and identified $CX_3CR1^{hi}Ly6C^{int}F4/80^{+}I\text{-}A/I\text{-}E^{+}$ macrophages, which we termed “arthritis-associated osteoclastogenic macrophages (AtoM)”, as the

OP-containing population in the arthritic joints, comprising a subset distinct from the BM OP-containing population[8,9,13]. We provided a detailed assessment of the differentiation trajectory of arthritic OPs, and tamoxifen-inducible FoxM1 deletion suppressed the capacity of AtoMs to differentiate into osteoclasts. We further demonstrated that synovial samples from RA patients contained $CX_3CR1^+HLA\text{-}DR^{hi}CD11c^+CD80^-CD86^+$ cells with osteoclastogenic potential and showed that osteoclastogenesis by these human cells was prevented by the FoxM1 inhibitor, thiostrepton. Collectively, these results demonstrate that AtoMs are the OP-containing population involved in articular bone erosion and that FoxM1 constitutes a potential target for RA treatment.

Results

Bone marrow-derived CX_3CR1^+ cells differentiate into osteoclasts in inflamed synovium.

To investigate the OP population in the inflamed synovium, we used a well-established experimental model, collagen-induced arthritis (CIA), in DBA1/J

mice. We elaborated an original protocol to expose the inflamed synovium on the bare area[11] of the femur by removing the patella, patellar ligaments, and quadriceps femoris muscles together under a stereoscopic microscope, and isolating the tissue using microscissors (Supplementary Fig. 1a, b). After removal of the Achilles tendon, isolation of the inflamed ankle joint synovium was possible (Supplementary Fig. 1c, d). CX_3CR1, a fractalkine receptor and marker for monocyte-lineage cells including BM-OPs under homeostatic conditions[8,13,14], was also able to mark OPs in the inflamed synovium *in vitro* (Fig. 1a). We then backcrossed CX_3CR1-EGFP knock-in mice and tartrate-resistant acid phosphatase (TRAP)-tdTomato transgenic mice onto the DBA1/J background to develop a reporter system for osteoclast differentiation in this model system. *Ex vivo* incubation of the inflamed synovium from double transgenic mice (CX_3CR1-EGFP/TRAP-tdTomato) showed that $EGFP^+$ cells gradually expressed tdTomato and underwent cell fusion to differentiate into osteoclasts, followed by a loss of CX_3CR1 expression (Fig. 1b and Supplementary Video. 1). $CX_3CR1^+TRAP^+$ cells that were in transition from OPs

to osteoclasts were detected at the pannus-bone interface *in vivo* (Fig. 1c). Together, these results suggest that EGFP$^+$ cells in the synovium contain OPs associated with arthritis.

As synovium-resident macrophages expressed CD11b[15] and CX_3CR1-EGFP (Supplementary Fig. 2a, b), we used BM chimeric mice with CX_3CR1-EGFP/TRAP-tdTomato hematopoietic cells to determine whether osteoclasts at the pannus–bone interface originate from the proliferation of local CX_3CR1^+ macrophages or newly recruited blood monocytes from BM. We used a non-linear optical process, second-harmonic generation (SHG), to distinguish synovial lining cells from BM cells by visualizing collagen-enriched bone matrices and synovial fibrous tissues (Supplementary Fig. 2a). After confirming that local EGFP$^+$ macrophages were radio-resistant (Supplementary Fig. 2c–e) and < 15% were replaced by BM cells 6 weeks after transplantation (Supplementary Fig. 2f–h), we induced CIA in the chimeric mice (Fig. 1d). The EGFP$^+$ cell frequencies in the inflamed synovium were equivalent between chimeric mice and control mice (Fig. 1f). In these chimeric mice, tdTomato$^+$

osteoclasts derived from the transplanted BM were detected at the pannus–bone interface (Supplementary Fig. 2i). Counting the frequencies of tdTomato$^+$ osteoclasts among total osteoclasts labelled by TRAP staining in wild-type/TRAP-tdTomato chimeras revealed that > 95% of the osteoclasts at the pannus–bone interface were derived from BM (Fig. 1g). Furthermore, an analysis of parabiotic mice involving wild-type and CX_3CR1-EGFP/TRAP-tdTomato mice paired for up to 2 months showed that > 40% of blood CX_3CR1^+ monocytes were exchanged between parabionts, although < 3% of synovial CX_3CR1^+ macrophages were exchanged under these physiological conditions (Supplementary Fig. 3a–c). When CIA was induced in both parabionts (Fig. 1e), EGFP$^+$ cells and tdTomato$^+$ osteoclasts were detected in pannus from wild-type parabionts, supporting the idea that the CX_3CR1^+ OPs and osteoclasts in pannus originated from cells in the blood circulation (Fig. 1h, i and Supplementary Fig. 3d).

$CX_3CR1^{hi}Ly6C^{int}F4/80^{hi}$I-A/I-E$^+$ macrophages in inflamed synovium have

high osteoclast differentiation potential.

To more specifically identify the subset origin of CX_3CR1^+ OPs, we performed a flow cytometric analysis of cells from the blood, BM, and synovium of CIA mice one week after the onset of arthritis. The frequencies and numbers of $CX_3CR1^{lo}Ly6C^{hi}$ cells (called “inflammatory monocytes”)[16] were significantly increased in the blood and BM of CIA mice (Fig. 2a, b). The inflamed synovium of CIA mice contained $CX_3CR1^{lo}Ly6C^{hi}$ cells, whereas $CX_3CR1^{hi}Ly6C^{-}$ cells (called “patrolling monocytes”)[16] were absent (Fig. 2c). Remarkably, there was a $CX_3CR1^{hi}Ly6C^{int}$ subset only in the CIA synovium. Because our chimeric data showed that the CX_3CR1^+ cells were almost all derived from blood, it is likely that $CX_3CR1^{lo}Ly6C^{hi}$ cells in the blood (R1) trans-migrated into the synovium (R2) and then differentiated into $CX_3CR1^{hi}Ly6C^{int}$ cells (R3) *in situ* (Fig. 2d). Indeed, inflamed synovium in wild-type parabionts, conjoined with CX_3CR1-EGFP mice, contained R3 cells, suggesting that such cells originated from a circulating population (Fig. 2e). Furthermore, when isolated R2 cells were labelled with CellTrace Violet and transferred into the inflamed knee joints of wild-type mice, >

70% of the transferred R2 cells differentiated into R3 cells (Fig. 2f). These results are consistent with our suggestion that R1 cells in the blood enter the inflamed synovium (R2) and differentiate into R3 cells. A phenotypic analysis revealed that the R3 cells were relatively large, F4/80^{hi}, I-A/I-E^{+}, CD11c^{lo}, and RANK^{dim}, and distinct from the OP-containing population in BM (BM-OPs) that have been characterised as being within the $CX_3CR1^{+}Ly6C^{hi}F4/80^{+}$ fraction[8,13] (Fig. 2g and Supplementary Fig. 4a). The R3 subset was sparse in other organs under both healthy and inflamed conditions, such as dextran sulphate sodium (DSS)-induced colitis (Supplementary Fig. 4b), suggesting that the R3 subset is tissue-restricted in its distribution with a high abundance in the inflamed synovium. Because R2 cells differentiate gradually into R3 cells *in situ*, both R2 and R3 fractions may contain transitional states. In fact, R2 and R3 cells constitute heterogeneous populations at least in terms of cellular size and granularity (reflected by the FSC/SSC); based on the F4/80 expression, we newly defined R3' ($CX_3CR1^{hi}Ly6C^{int}$F4/80^{hi}) as "fully differentiated R3" for further analyses (Supplementary Fig. 5). Similarly, we defined R2'

(CX$_3$CR1^{lo}Ly6C^{hi}F4/80^{int}) as “basal state R2”. May–Giemsa staining showed that the R3’ cells had an abundant foamy cytoplasm and cytoplasmic vacuoles, representing a macrophage morphology (Fig. 2h). In contrast, R2’ cells had peripherally located kidney-shaped nuclei, indicating that differentiation to the macrophage state is not obligatory for monocytes after entry into the synovium without an additional trigger. When stimulated directly with RANKL, R3’ cells readily differentiated into osteoclasts that resorbed inorganic crystalline calcium phosphate *in vitro* (Fig. 2i), suggesting that R3’ cells contain functional OPs in the inflamed synovium; therefore, we designated these cells as AtoMs. The proportion and osteoclastogenic potential of R3 cells were comparable in the knee and ankle joints (Supplementary Fig. 6a, b). Although the BM also contained a small population of CX$_3$CR1^{hi}Ly6C^{int} cells with the potential to form osteoclasts, May−Giemsa staining of these cells showed cells with diameters of 8−12 μm and peripherally located kidney-shaped nuclei (Supplementary Fig. 4c, d), which is the characteristic monocyte morphology. This is explained by a previous observation that CX$_3$CR1^{hi}Ly6C^{-} monocytes are derived from

$CX_3CR1^{lo}Ly6C^{hi}$ monocytes in the BM[17], and $CX_3CR1^{hi}Ly6C^{int}$ cells in the BM may be in transition from $Ly6C^{hi}$ monocytes to $Ly6C^{-}$ monocytes, indicating that $CX_3CR1^{hi}Ly6C^{int}$ cells in the BM are distinct from inflamed synovium R3 cells.

The RANKL-RANK-OPG axis is essential for R3' cell osteoclastogenesis.

Previous studies reported that TNF−α and IL−6 drive osteoclast formation in BM-derived macrophages (BMM) *in vitro*, suggesting the presence of a RANKL-independent pathway of osteoclastogenesis[18,19]. Therefore, we examined whether R3' cells from the inflamed synovium can differentiate into osteoclasts without RANKL. The results showed that TNF−α and IL−6 minimally induced osteoclasts from R3' cells, as compared to RANKL (Fig. 3a, b). In contrast, simultaneous addition of TNF−α and RANKL significantly promoted RANKL-induced osteoclastogenesis (Fig. 3a, b). Previous studies showed that TNF−α did not enhance osteoclastogenesis in BMM when added simultaneously with RANKL. However, RANKL priming several days prior to addition of TNF−α induced maximal osteoclastogenesis[20,21]. Collectively, these results imply that

R3’ cells were already primed by RANKL in the pannus microenvironment. Furthermore, IL−6 was reported to trigger osteoclast formation together with soluble IL−6 receptor in BM cells[22]. However, IL−6 inhibited RANKL-induced osteoclastogenesis of R3’ cells (Fig. 3a, b). Considering that RANKL-RANK signaling is essential for osteoclastogenesis of R3’ cells, we examined the effect of the decoy-receptor osteoprotegerin (OPG), which showed dose-dependent inhibition of osteoclastogenesis induced by RANKL or RANKL plus TNF−α (Fig. 3c, d).

Transcriptional profiling by RNA sequencing (RNA-Seq) identifies FoxM1 as one of the key regulators of R3’ cells.

We next performed an unbiased global transcriptomic comparison of R1, R2’, and R3’ cells by RNA-Seq. Principal component analysis (PCA) showed tight clustering across replicates, indicating that R1–3’ cells constitute distinct, reproducible subsets (Fig. 4a). Based on the top 300 upregulated genes, we found that R2’ cells had higher expression levels of transcripts encoding

chemokines (*Cxcl1*, *Cxcl2*, *Ccl2*, *Ccl3*, and *Ccl4*), inflammatory cytokines (*Il1*, *Il6*, and *Tnf*), and *Vegfa* than R1 cells (Fig. 4b). In contrast, R3' cells showed preferential expression of osteoclast marker genes (*Ctsk*, *Acp5*, *Mmp9*, *Atp6v0d2*, and *Ppargc1b*) (Fig. 4c, d), and a gene-set enrichment analysis (GSEA) showed the enrichment of genes associated with osteoclast differentiation ($p = 0.0123$), mitochondrial translation ($p < 0.0001$), and oxidative phosphorylation ($p < 0.0001$), compared to R2' cells (Fig. 4e, Supplementary Fig. 7c, and Supplementary Table 1). To determine the transcription factors responsible for regulating the osteoclastogenic potential of R3' cells, we generated a global mRNA expression profile of transcription factors increased in the R3' subset and predicted upstream regulators with QIAGEN's Ingenuity Pathway Analysis. The predicted regulator with the top Z-score was FoxM1 ($p = 9.77E^{-19}$) (Fig. 4f and Supplementary Fig. 7d), which was increased by 11.69-fold; this upregulation was validated at both the mRNA and protein levels (Fig. 4g, h). E2F1, which was reported previously to promote osteoclastogenesis

under inflammatory conditions[23], was detected as a predicted regulator with the second highest Z-score ($p = 9.22E^{-21}$).

FoxM1 is a multifaceted transcription factor with diverse and cell type-specific functions *in vivo*[24]. In adult tissues, FoxM1 plays a prominent role in carcinogenesis by inducing the epithelial–mesenchymal transition, a process that renders tumour cells more aggressive and invasive[24], leading to metastasis[25]. Because the invasive phenotype of a tumour is analogous to pannus in arthritis, which erodes the bone surface to destroy joints, these correlations prompted us to explore the function of FoxM1 in arthritis. A natural product, thiostrepton, interacts directly with FoxM1 and inhibits its binding to genomic target sites[26]. Thiostrepton also prevents FoxM1 from binding to and activating its own promoter, disrupting the positive auto-regulatory loop[27] without being cytotoxic in untransformed cells[28]. The treatment of R3' cells with thiostrepton resulted in the efficient attenuation of FoxM1 expression in a dose-dependent manner (Fig. 4i) without inducing apoptosis or inhibiting cell proliferation at concentrations ≤ 1 μM (Supplementary Fig. 8a, b). Thiostrepton

inhibited the osteoclastogenesis of R3' cells significantly *in vitro* (Fig. 4j), and attenuated articular bone erosion *in vivo* (Fig. 4l, m and Supplementary Fig. 9a–d). Thiostrepton partially reduced the arthritic scores of CIA mice (Fig. 4k) and inhibited inflammatory cytokine expression in the synovium (Supplementary Fig. 8c), which may indirectly protect against bone erosion. To elucidate the effect of thiostrepton on homeostatic bone remodelling, we injected 50 mg/kg thiostrepton twice a week for 5 weeks. Body growth and bone morphology did not differ between vehicle- and thiostrepton-treated groups, indicating that thiostrepton does not affect homeostatic bone remodeling *in vitro* or *in vivo* (Supplementary Fig. 8d-h). These results show that FoxM1 is involved in the osteoclastogenic potential of R3' cells in arthritis.

Single cell RNA-sequencing analysis identifies highly osteoclastogenic population in synovial R3 cells

Since only a portion of inflamed synovium cells differentiate into osteoclasts *in vivo*, we hypothesized the presence of a specific subpopulation in R3 cells,

which is in transition from OPs to osteoclasts on articular bone surfaces. To identify and characterize the population, we sorted R3 cells from inflamed knee synovium one week after CIA onset and conducted single cell RNA-sequencing analysis (Fig. 5a). A total of 8,682 R3 cell transcriptomes were analyzed and hierarchically clustered using t-distributed stochastic neighbor embedding (t-SNE) (Fig. 5b). Among the four R3 cell clusters, P1 exhibited the osteoclastogenic phenotype, constituting 10.2 % of R3 cells. The expression levels of osteoclast related genes, such as *Acp5* (encoding TRAP), *Ctsk, Atp6v0d2, Mmp9,* and *Itgb3* were, respectively, 56.4, 72.1, 65.3, 147, and 144 times higher in the P1 cluster, as compared to the rest of the cell clusters (Fig. 5c, d). Chemokines, chemokine receptors, and inflammatory cytokines, such as *Tnf*, were preferentially expressed in the other clusters relative to P1 (Fig. 5c, d). The expression level of *FoxM1* was 17.1 times higher in P1, as compared to the other clusters, supporting its role as a regulator of osteoclastogenesis in a specific cell type of the inflamed synovium (Fig. 5c, d).

M-CSF mediates R2 to R3 transition and upregulates FoxM1 expression

To identify the cytokine(s) responsible for upregulating FoxM1 expression from R2 to R3 cells, we sorted R2 cells from the inflamed synovium and incubated them with M-CSF and RANKL, the cytokines essential for osteoclastogenesis[5,6,29], or inflammatory cytokines, such as TNF-α and IL-6. The results showed that M-CSF alone upregulated FoxM1 expression (Fig. 6a) and triggered differentiation into R3 cells (Fig. 6b), potentially explaining the protective effect of an M-CSF deletion on bone erosion in arthritis[30,31]. In contrast, RANKL, TNF-α, IL-6, and the combination of TNF-α/IL-6 had no additive effect with M-CSF, and adhesion was dispensable for FoxM1 upregulation (Fig. 6a). Consistent with previous studies showing that inflammatory cytokines stimulate the production of M-CSF from synovial fibroblasts[32], chondrocytes[33], and endothelial cells[34], the M-CSF expression levels were higher in inflamed synovium than in BM and healthy synovium, signifying an arthritis-specific environment that could promote erosive events (Fig. 6c, d). Although overexpression of FoxM1 did not induce spontaneous osteoclast formation

(Supplementary Fig. 10a-c), the minimum dose of M-CSF required for RANKL-induced osteoclastogenesis was lower in macrophages overexpressing FoxM1, supporting its role in partially replacing the contribution of M-CSF to osteoclastogenesis (Supplementary Fig. 10d, e).

The source of key cytokines in inflamed synovium was further examined by isolating leukocytes (Lin^+CD45^+ cells), endothelial cells ($Lin^-CD45^-CD31^+CD140a^-$ cells), and fibroblasts ($Lin^-CD45^-CD140a^+CD31^-$ cells) from CIA synovium (Fig. 6e). The expression of M-CSF was higher in fibroblasts and leukocytes, as compared to endothelial cells, while RANKL expression in fibroblasts was about 400 times higher than in leukocytes and endothelial cells (Fig. 6f). Among inflammatory cytokines, the expression of IL-6 was highest in fibroblasts and TNF was highest in leukocytes (Fig. 6f).

We next examined whether FoxM1 expression levels differ between R3 cells and mature osteoclasts. Approximately 40% of the R3 cells seeded on the plate differentiated into osteoclasts (Supplementary Fig. 11a). Resultant mononuclear cells and multinucleated mature osteoclasts were isolated from the

temperature-responsive cell cultureware, RepCell (Supplementary Fig. 11b), and $FSC^{hi}SSC^{hi}$TRAP-tdtomato^{+} multinucleated osteoclasts were sorted as described previously[10], with slight modifications (Supplementary Fig. 11c). FoxM1 expression was comparable between R3 cells and mature osteoclasts (Supplementary Fig. 11d), indicating that multinucleation does not upregulate FoxM1 expression.

FoxM1 contributes to arthritis-induced bone destruction

We next analyzed the effects of the FoxM1 time-specific deletion in $FoxM1^{fl/fl}Rosa26^{CreERT2}$ mice. Since C57BL/6 (B6) mice were resistant to reliable CIA induction, we used the collagen antibody-induced arthritis (CAIA) model. We found that R3' cells with high FoxM1 expression levels also developed under these conditions and that arthritis was consistently induced in B6 mice[35] (Supplementary Fig. 12a–c). The *in vivo* injection of tamoxifen efficiently deleted FoxM1 genes (Fig. 7a, b), and the suppression of FoxM1 expression was most significant in CX_3CR1^{+} macrophages (Fig. 7c). FoxM1 deletion partially inhibited

synovial R3 cell osteoclastogenesis *in vitro* (Fig. 7d) without inducing apoptosis (Fig. 7e), or altering TNF−α expression (Fig. 7f). FoxM1 deletion mitigated bone erosion *in vivo*, which was partly reversed by the adoptive transfer of $FoxM1^{+/+}CX_3CR1^{+}$ monocytes but not by $FoxM1^{-/-}CX_3CR1^{+}$ monocytes (Fig. 7g and Supplementary Fig. 13a, b). The arthritic score was also reduced by the global FoxM1 deletion (Fig. 7h). By contrast, osteoclastogenesis by BM-OPs was not affected by the FoxM1 deletion *in vitro* (Fig. 7d). Myeloid cell-specific FoxM1 knockout mice (LysM-Cre:$FoxM1^{fl/fl}$) and global deletion beginning at 6 weeks of age resulted in no change in body growth or physiological bone remodelling (Supplementary Figs. 14 and 15).

To clarify the role of FoxM1 in the conversion of R2 into R3 cells, we sorted R2 cells from CAIA mice treated with or without tamoxifen (Supplementary Fig. 16a). Incubation with M-CSF successfully converted R2 cells into R3 cells in both groups ($FoxM1^{+/+}$ and $FoxM1^{-/-}$), indicating that FoxM1 is dispensable for upregulation of CX_3CR1 and downregulation of Ly6C (Supplementary Fig. 16b).

RA synovial $CX_3CR1^+HLA\text{-}DR^{hi}CD11c^+CD86^+$ cells have high osteoclastogenic potential

Finally, we examined the relevance of the osteoclastogenesis mechanism in humans. Because Ly6C is not expressed in human cells, we used CX_3CR1 and HLA-DR (I-A/I-E in mice) to identify the subset with high osteoclastogenic potential. We detected $CX_3CR1^+HLA\text{-}DR^{hi}CD14^+CD64^+$ cells[36] in the synovial fluid and synovium, but not in blood, of RA patients (Fig. 8a). Given that these cells from synovial fluid and synovium of RA patients were negative for CD80, positive for CD11c, and partially positive for CD86 (Fig. 8b), we further divided $CX_3CR1^+HLA\text{-}DR^{hi}$ cells into $CX_3CR1^+HLA\text{-}DR^{hi}CD11c^+CD86^-$ cells (P1) and $CX_3CR1^+HLA\text{-}DR^{hi}CD11c^+CD86^+$ cells (P2) (Fig. 8c). P2 cells had higher potential for osteoclast formation and FoxM1 expression compared with P1 cells (Fig. 8d, e) and thiostrepton significantly inhibited osteoclastogenesis by these cells (Fig. 8f). Because P1 and P2 cells express CD86 over a continuous range of values, without a clear threshold separating distinct subpopulations, some of

the P1 cells with relatively high FoxM1 expression also formed osteoclasts (Fig. 8g), and this was inhibited by thiostrepton (Fig. 8f).

Discussion

In this report, we provided a detailed assessment of the differentiation trajectory of inflammatory OPs (Supplementary Fig. 17), and identified a distinct arthritis-associated macrophage population, AtoM, which is responsible for articular bone erosion in pannus. Although extensive studies have identified monocytoid cells with osteoclastogenic potential in the BM or spleen under various conditions[8,9,10,13,37], pathogenic osteoclasts formed on the pannus–bone interface are derived from circulating blood monocytes which ingress into the synovium, and a precise analysis of the inflamed synovium is indispensable to identify the *in situ* OP population in the arthritic condition. Our protocol succeeded in isolating the inflamed synovium on the bare area[11], which can be confirmed by its unique flow cytometric plots compared with those of other organs (Supplementary Fig. 4b). We also demonstrated that

CD45^{+}CX$_3$CR1^{lo}Ly6C^{hi} populations in the blood (R1) and inflamed synovium (R2) have substantially distinct transcriptional profiles in terms of chemokines (*Cxcl1*, *Cxcl2*, *Ccl2*, *Ccl3*, and *Ccl4*) and inflammatory cytokines (*Il1*, *Il6*, and *Tnf*). Distinguishing synovial cells from BM cells enabled us to identify a unique macrophage population, AtoM, suggesting that macrophage subtypes *in vivo* should be defined depending on the residing organs and corresponding diseases, rather than the simple terminology of M1 and M2 macrophages.

Notably, AtoMs highly express several cell surface molecules for antigen presentation, including MHC class II and CD80/86 (Fig. 2g). Despite its controversy, this result may suggest that osteoclasts in arthritic joints derived from AtoMs are involved in antigen presentation in local foci. A previous study of inflammatory bowel disease reported that osteoclasts generated under inflammatory conditions are efficient at inducing TNF-α-producing CD4^{+} T cells, amplifying both the inflammatory response and bone destruction[10]. Other studies have also demonstrated that dendritic cells (DCs) can differentiate into osteoclasts under inflammatory conditions[38,39]. Although the F4/80 expression

and structural phenotype of AtoMs (e.g., vacuolar cytoplasm) suggest that they can be classified as macrophages, the expression of DC markers such as CD11c and MHC class II imply that AtoMs may share functional characteristics with both macrophages and DCs.

FoxM1 plays a prominent role in carcinogenesis by rendering tumour cells more aggressive and invasive[24]; however, it has never been reported in the context of autoimmune diseases. A previous study showed that FoxM1 directly drives mitochondrial biogenesis[40], which is crucial for differentiation into osteoclasts[41], and our RNA-Seq data are consistent with this finding, in that AtoMs were significantly enriched with genes associated with mitochondrial translation and oxidative phosphorylation (Supplementary Fig. 7c). Thus, FoxM1 may play a role in AtoMs by meeting the high energy demand for osteoclastogenesis under arthritic conditions. Because global FoxM1 inhibition alleviated not only articular bone destruction but also inflammation, it is possible that other cells outside of the myeloid lineage influence the inflammatory process via FoxM1, which can indirectly affect bone destruction. Future studies

are needed to advance our knowledge on this subject.

In human cells, several studies have reported that macrophages in the synovial fluid and synovium of RA patients express CX_3CR1[42–44]; HLA-DR has also been used to categorize human blood monocytes[16]. Because mouse AtoMs express CX_3CR1 and I-A/I-E, the application of these two markers in samples from RA patients facilitated identification of the $CX_3CR1^{+}HLA\text{-}DR^{hi}$ population only in the synovial samples and we further revealed that human synovial OPs were included in the $CX_3CR1^{+}HLA\text{-}DR^{hi}CD11c^{+}CD86^{+}$ population. An anti-fractalkine monoclonal antibody phase-1/2 clinical trial demonstrated an effective clinical response in active RA patients[45], and further analysis of osteoclastogenesis and chemotactic activity in these cells may improve our understanding of its pathophysiology in RA.

Our protocol allows for the precise isolation of inflamed synovium from arthritic mice and may facilitate investigations to determine the role of other immune cells involved in pannus *in situ*, including lymphocytes, fibroblasts, and endothelial cells. In addition, although cytokine-inhibiting biological agents in

current clinical use have drawbacks related to increased susceptibility to infection, the direct targeting of FoxM1 may facilitate the development of pathogenic osteoclast-targeted treatment. This is distinct from therapies targeting CX_3CL1 (fractalkine) because CX_3CR1^+ cells do not necessarily depend on the CX_3CL1-CX_3CR1 axis for chemotaxis within the synovial tissue and chemotaxis is not directly involved in osteoclastogenesis. Furthermore, pathological bone destruction represents a final common pathway in several chronic inflammatory disorders, including histiocytosis, spondyloarthritis, and sarcoidosis, which are responsible for substantial disability and morbidity[6]. The identification of arthritis-associated OPs implies that the resultant osteoclasts are more heterogeneous than presently thought, and an understanding of the dynamics of pathological osteoclastogenesis should prompt the development of optimized treatment for inflammatory bone destruction.

1. Pirzgalska, R. M. *et al.* Sympathetic neuron-associated macrophages contribute to obesity by importing and metabolizing norepinephrine. *Nat.*

Med. **23**, 1309–1318 (2017).

2. Okabe, Y. & Medzhitov, R. Tissue-specific signals control reversible program of localization and functional polarization of macrophages. *Cell* **157**, 832–844 (2014).

3. Satoh, T. *et al.* Identification of an atypical monocyte and committed progenitor involved in fibrosis. *Nature* **541**, 96–101 (2017).

4. Asano, K. *et al.* CD169-positive macrophages dominate antitumor immunity by crosspresenting dead cell-associated antigens. *Immunity* **34**, 85–95 (2011).

5. Arai, F. *et al.* Commitment and differentiation of osteoclast precursor cells by the sequential expression of c-fms and receptor activator of nuclear factor κb (Rank) receptors. *J. Exp. Med.* **190**, 1741–1754 (2002).

6. Schett, G. & Gravallese, E. Bone erosion in rheumatoid arthritis: Mechanisms, diagnosis and treatment. *Nat. Rev. Rheumatol.* **8**, 656–664 (2012).

7. McInnes, I. The pathogenesis of rheumatoid arthritis. *N. Engl. J. Med.* **365**,

2205–19 (2011).

8. Charles, J. F. *et al.* Inflammatory arthritis increases mouse osteoclast precursors with myeloid suppressor function. *J. Clin. Invest.* **122**, 4592–4605 (2012).

9. Seeling, M. *et al.* Inflammatory monocytes and Fc receptor IV on osteoclasts are critical for bone destruction during inflammatory arthritis in mice. *Proc. Natl. Acad. Sci.* **110**, 10729–10734 (2013).

10. Ibáñez, L. *et al.* Inflammatory osteoclasts prime TNFα-producing CD4+ T cells and express CX3CR1. *J. Bone Miner. Res.* **31**, 1899–1908 (2016).

11. Werner, D. *et al.* Early changes of the cortical micro-channel system in the bare area of the joints of patients with rheumatoid arthritis. *Arthritis Rheumatol.* **69**, 1580–1587 (2017).

12. Adamopoulos, I. E. & Mellins, E. D. Alternative pathways of osteoclastogenesis in inflammatory arthritis. *Nat. Rev. Rheumatol.* **11**, 189–194 (2015).

13. Jacome-Galarza, C. E., Lee, S. K., Lorenzo, J. A. & Aguila, H. L.

Identification, characterization, and isolation of a common progenitor for osteoclasts, macrophages, and dendritic cells from murine bone marrow and periphery. *J. Bone Miner. Res.* **28**, 1203–1213 (2013).

14. Ishii, M. *et al.* Sphingosine-1-phosphate mobilizes osteoclast precursors and regulates bone homeostasis. *Nature* **458**, 524–528 (2009).

15. Misharin, A. V *et al.* Non-classical Ly6C− monocytes drive the development of inflammatory arthritis in mice. *Cell Rep.* **9**, 591–604 (2014).

16. Geissmann, F., Jung, S. & Littman, D. R. Blood monocytes consist of two principal subsets with distinct migratory properties. *Immunity* **19**, 71–82 (2003).

17. Yona, S. *et al.* Fate mapping reveals origins and dynamics of monocytes and tissue macrophages under homeostasis. *Immunity* **38**, 79–91 (2013).

18. Yokota, K. *et al.* Combination of tumor necrosis factor α and interleukin-6 induces mouse osteoclast-like cells with bone resorption activity both in vitro and in vivo. *Arthritis Rheumatol.* **66**, 121–129 (2014).

19. O'Brien, W. *et al.* RANK-independent osteoclast formation and bone

erosion in inflammatory arthritis. *Arthritis Rheumatol.* **68**, 2889–2900 (2016).

20. Lam, J. *et al.* TNF-α induces osteoclastogenesis by direct stimulation of macrophages exposed to permissive levels of RANK ligand. *J. Clin. Invest.* **106**, 1481–1488 (2000).

21. Ochi, S. *et al.* Pathological role of osteoclast costimulation in arthritis-induced bone loss. *Proc. Natl. Acad. Sci.* **104**, 11394–11399 (2007).

22. Tamura, T. *et al.* Soluble interleukin-6 receptor triggers osteoclast formation by interleukin 6. *Proc. Natl. Acad. Sci.* **90**, 11924–11928 (2006).

23. Murata, K. *et al.* Hypoxia-sensitive COMMD1 integrates signaling and cellular metabolism in human macrophages and suppresses osteoclastogenesis. *Immunity* **47**, 66–79 (2017).

24. Lam, E. W.-F., Brosens, J. J., Gomes, A. R. & Koo, C.-Y. Forkhead box proteins: tuning forks for transcriptional harmony. *Nat. Rev. Cancer* **13**, 482–495 (2013).

25. Wang, Z., Banerjee, S., Kong, D., Li, Y. & Sarkar, F. H. Down-regulation of Forkhead Box M1 transcription factor leads to the inhibition of invasion and angiogenesis of pancreatic cancer cells. *Cancer Res.* **67**, 8293–8300 (2007).

26. Hegde, N. S., Sanders, D. A., Rodriguez, R. & Balasubramanian, S. The transcription factor FOXM1 is a cellular target of the natural product thiostrepton. *Nat. Chem.* **3**, 725–731 (2011).

27. Halasi, M. & Gartel, A. L. A novel mode of FoxM1 regulation: Positive auto-regulatory loop. *Cell Cycle* **8**, 1966–1967 (2009).

28. Kwok, J. M.-M. *et al.* Thiostrepton selectively targets breast cancer cells through inhibition of forkhead box M1 expression. *Mol. Cancer Ther.* **7**, 2022–2032 (2008).

29. Mbalaviele, G., Novack, D. V., Schett, G. & Teitelbaum, S. L. Inflammatory osteolysis: A conspiracy against bone. *J. Clin. Invest* **127**, 2030–2039 (2017).

30. Campbell, I. K., Rich, M. J., Bischof, R. J. & Hamilton, J. A. The

colony-stimulating factors and collagen-induced arthritis: exacerbation of disease by M-CSF and G-CSF and requirement for endogenous M-CSF. *J. Leukoc. Biol.* **68**, 144–150 (2000).

31. Ando, W. *et al.* Imatinib mesylate inhibits osteoclastogenesis and joint destruction in rats with collagen-induced arthritis (CIA). *J. Bone Miner. Metab.* **24**, 274–282 (2006).

32. Hamilton, J. A. Colony-stimulating factors in inflammation and autoimmunity. *Nat. Rev. Immunol.* **8**, 533–544 (2008).

33. Campbell, I. K., Ianches, G. & Hamilton, J. A. Production of macrophage colony-stimulating factor (M-CSF) by human articular cartilage and chondrocytes. Modulation by interleukin-1 and tumor necrosis factor α. *Biochim Biophys Acta* **1182**, 57–63 (1993).

34. Nakano, K. *et al.* Rheumatoid synovial endothelial cells produce macrophage colony-stimulating factor leading to osteoclastogenesis in rheumatoid arthritis. *Rheumatology* **46**, 597–603 (2007).

35. Hutamekalin, P. *et al.* Collagen antibody-induced arthritis in mice:

Development of a new arthritogenic 5-clone cocktail of monoclonal anti-type II collagen antibodies. *J. Immunol. Methods* **343**, 49–55 (2009).

36. Xue, J. *et al.* Transcriptome-based network analysis reveals a spectrum model of human macrophage activation. *Immunity* **40**, 274–288 (2014).

37. Šućur, A. *et al.* Induction of osteoclast progenitors in inflammatory conditions: Key to bone destruction in arthritis. *Int. Orthop.* **38**, 1893–1903 (2014).

38. Wakkach, A. *et al.* Bone marrow microenvironment controls the in vivo differentiation of murine dendritic cells into osteoclasts. *Blood* **112**, 5074–5083 (2008).

39. Rivollier, A. *et al.* Immature dendritic cell transdifferentiation into osteoclasts: A novel pathway sustained by the rheumatoid arthritis microenvironment. *Blood* **104**, 4029–4037 (2004).

40. De Luca, A. *et al.* Mitochondrial biogenesis is required for the anchorage-independent survival and propagation of stem-like cancer cells. *Oncotarget* **6**, 14777–95 (2015).

41. Ishii, K. A. *et al.* Coordination of PGC-1β and iron uptake in mitochondrial biogenesis and osteoclast activation. *Nat. Med.* **15**, 259–266 (2009).

42. Ruth, J. H. *et al.* Fractalkine, a novel chemokine in rheumatoid arthritis and in rat adjuvant-induced arthritis. *Arthritis Rheum.* **44**, 1568–1581 (2001).

43. Blaschke, S. *et al.* Proinflammatory role of fractalkine (CX3CL1) in rheumatoid arthritis. *J. Rheumatol.* **30**, 1918–1927 (2003).

44. Nanki, T., Imai, T. & Kawai, S. Fractalkine/CX3CL1 in rheumatoid arthritis. *Mod. Rheumatol.* **7595**, 1–6 (2016).

45. Tanaka, Y. *et al.* Safety, pharmacokinetics, and efficacy of E6011, an antifractalkine monoclonal antibody, in a first-in-patient phase 1/2 study on rheumatoid arthritis. *Mod. Rheumatol.* **28**, 58–65 (2018).

Acknowledgements

We thank Dr. Ronald N. Germain (NIAID/NIH, USA) for critically reviewing this manuscript. This work was supported by CREST, Japan Science and Technology Agency; Grants-in-Aid for Scientific Research (S) from the Japan Society for the Promotion of Science (JSPS to M.I.); Grant-in-Aid for Young

Scientists (A) from JSPS (to J.K.); grants from the Uehara Memorial Foundation (to M.I.); from the Kanae Foundation for the Promotion of Medical Sciences (to M.I.); from Mochida Memorial Foundation (to M.I.); and from the Takeda Science Foundation (to M.I.). The English in this document has been checked by at least two professional editors, both native speakers of English. For a certificate, please see: http://www.textcheck.com/certificate/576gzq

Author contributions

T.H and M.I. conceived the study. T.H and J.K designed the experiments. T.S, Y.M, S.S, T.M, K.Y, and T.T discussed the experiments and results. K.E and M.H provided the samples from RA patients. Y.Y, A.H, and V.K provided the FoxM1$^{fl/fl}$ mouse line and A.H provided the RosaERT2Cre mouse line. D.O performed the RNA-seq analysis and single cell RNA-seq analysis. T.H wrote the initial draft. J.K and M.I. revised the final draft.

Competing interests

The authors declare no competing interests.

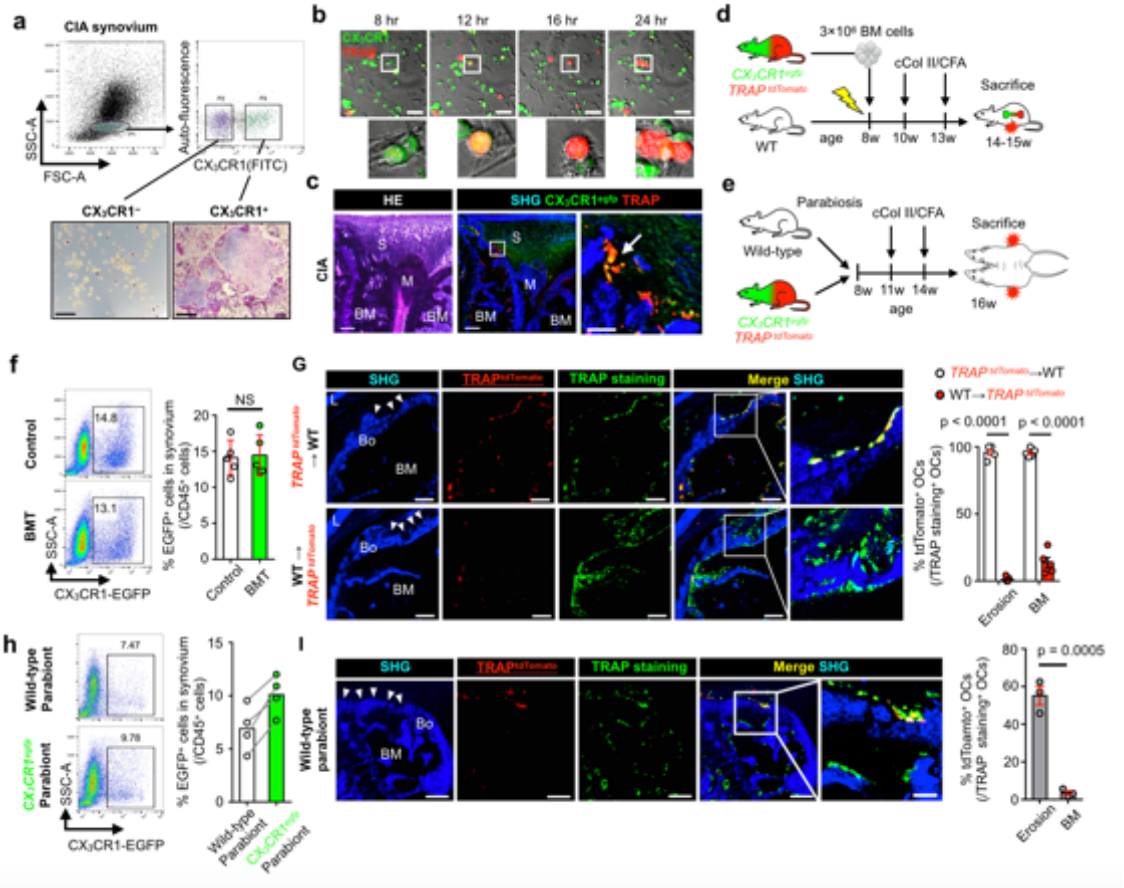

Figure 1. Bone marrow-derived CX_3CR1^+ cells differentiate into osteoclasts in pannus.

a, *In vitro* differentiation of CX_3CR1^+ cells isolated from inflamed synovium of knee joints into OC-like cells upon RANKL stimulation. Bars, 100 μm

b, *Ex vivo* incubation of inflamed synovium of knee joints from double transgenic mice (CX_3CR1-EGFP/TRAP-tdTomato) upon RANKL stimulation. Enlargement of the boxed areas are displayed. Bars, 50 μm.

c, Representative confocal images of arthritic knee joints from CX_3CR1-EGFP transgenic mice with TRAP staining. The arrowhead indicates merged osteoclasts. BM: bone marrow, M: meniscus, S: synovium. Bars, 200 and 30 μm.

d, Schematic diagram showing the experimental design for bone marrow chimeric mice, and **e,** parabiotic mice with CIA.

f, Flow cytometry plots and cumulative data of CX_3CR1-EGFP$^+$ cells from inflamed knee joints of CX_3CR1-EGFP transgenic mice (control) and bone marrow chimeric mice (BMT).

g, Representative confocal images and frequencies of TRAP-tdTomato$^+$ osteoclasts among TRAP staining$^+$ osteoclasts in the inflamed knee joints of indicated chimeras. Bars, 200 μm.

h, Flow cytometry plots and cumulative data of CX_3CR1-EGFP$^+$ cells from inflamed knee joints of indicated parabionts.

i, Representative confocal images and frequencies of TRAP-tdTomato$^+$ osteoclasts among TRAP staining$^+$ osteoclasts in the inflamed knee joints of indicated parabionts. Bars, 150 and 50 μm.

Unpaired two-tailed *t* test (f, g, i). Mean ± S.E.M. for each group. Symbols represent individual mice.

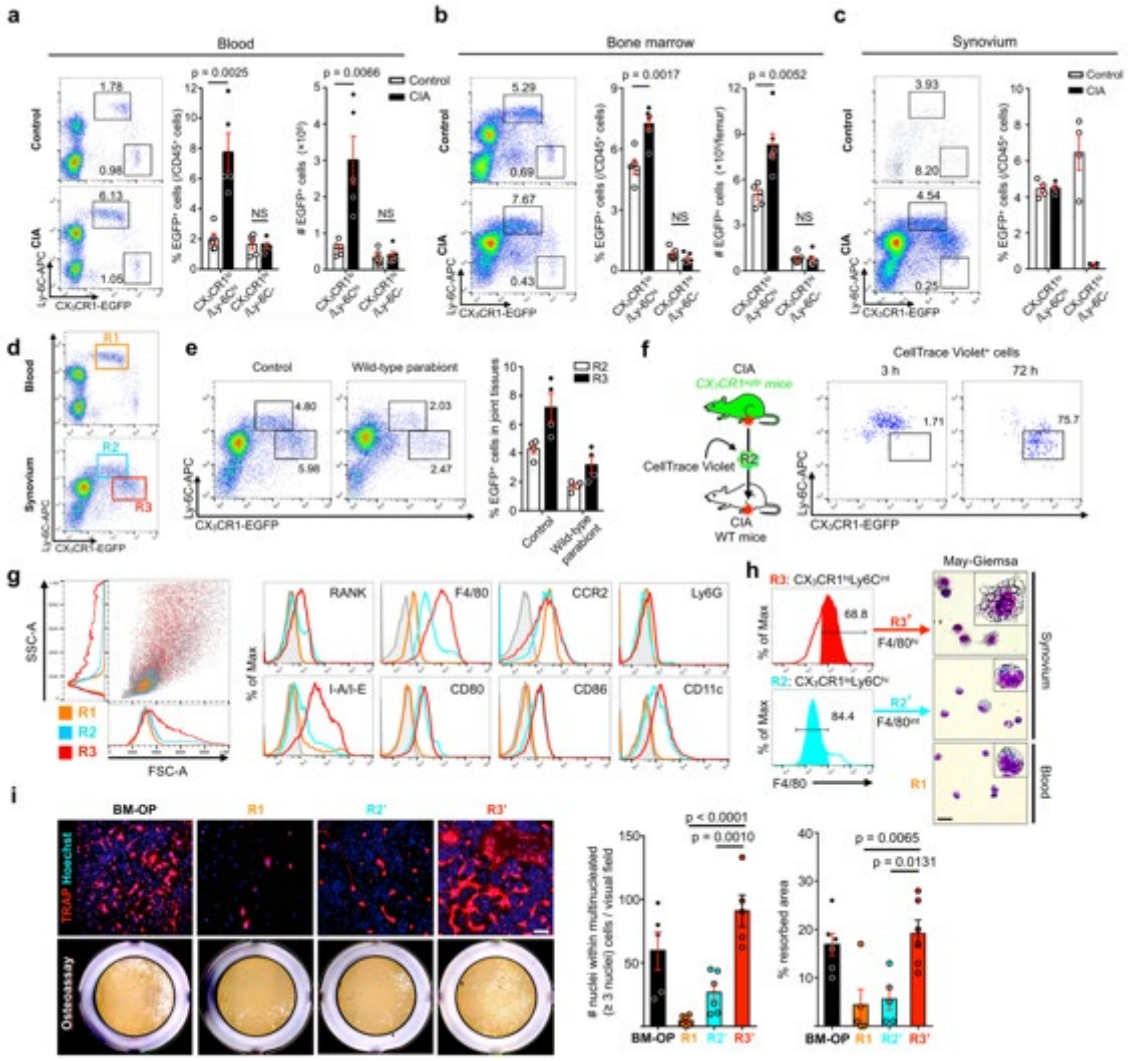

Figure 2. $CX_3CR1^{hi}Ly6C^{int}F4/80^{hi}I\text{-}A/I\text{-}E^{+}$ macrophages in the inflamed synovium have high osteoclast differentiation potential.

a–c, Representative plots and quantification of $CX_3CR1\text{-}EGFP^{+}$ cells in the blood, bone marrow, and knee joints of control and CIA mice 1 week after arthritis onset.

d, Definitions of R1, R2, and R3 cells in the blood and synovium of CIA mice.

e, Detection of R2 and R3 cells in the CIA knee synovium of wild-type (WT) parabionts paired with CX_3CR1-EGFP transgenic mice.

f. Adoptive transfer of CellTrace Violet-labelled R2 cells from the inflamed knee synovium of CX_3CR1-EGFP transgenic mice into the inflamed knee joints of WT mice.

g, FACS-based phenotypic characterization of R1, R2, and R3 cells with indicated cell surface markers. Shaded regions indicate staining with isotype controls. Dot plots of FSC-A/SSC-A are displayed with an overlay of R1 cells from blood, and R2 and R3 cells from knee synovium.

h, Morphological assessment of R1, R2', and R3' cells with May–Giemsa staining. Bar, 20 μm.

i, Osteoclast differentiation and resorption potential of R1, R2', R3' cells, and OP-containing population from bone marrow (BM-OPs). R1, R2', R3' cells, and BM-OPs were sorted and directly stimulated with 100 ng/ml RANKL and 10 ng/ml M-CSF for 6 days.

Unpaired two-tailed *t* test (a–c) and one-way ANOVA with Bonferroni's post hoc

test (i). Mean ± S.E.M. for each group. Symbols represent individual mice except for the control group in **c**, where multiple mice were used for a single symbol because of the limited number of cells in the uninflamed condition.

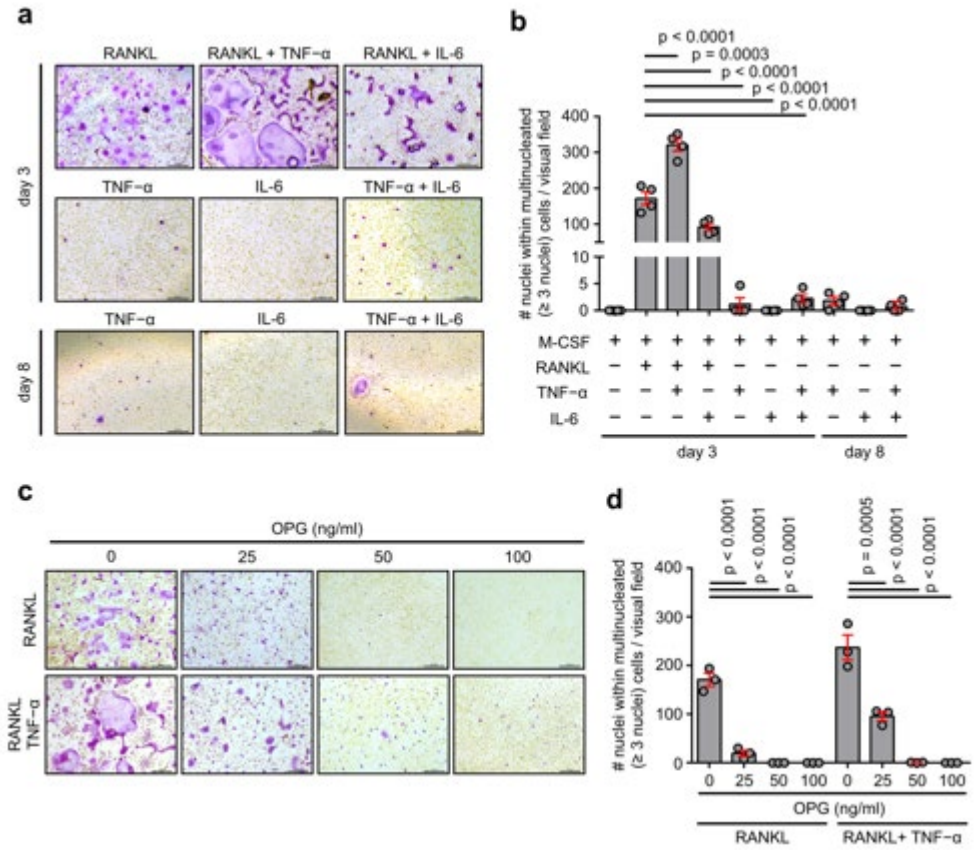

Figure 3. The RANKL-RANK-OPG axis is essential for R3' cell osteoclastogenesis.

a. Representative TRAP staining images of synovial R3' cells from knee and ankle joints cultured with 10 ng/ml M-CSF, 50 ng/ml RANKL, 50 ng/ml TNF−α, or 50 ng/ml IL-6, either alone or in combination. Bars, 200 μm.

b, Quantification of nuclei within multinucleated cells within the visual field in **a**.

c, Representative TRAP staining images of R3’ cells cultured with 10 ng/ml M-CSF, 50 ng/ml RANKL, and 50 ng/ml TNF−α with osteoprotegerin (OPG) at the indicated concentrations. Bars, 200 μm.

d, Quantification of nuclei within multinucleated cells within the visual field in **c**.

One-way ANOVA test with Bonferroni post-hoc test (b, d). Mean ± s.e.m. for each group. Symbols represent individual mice.

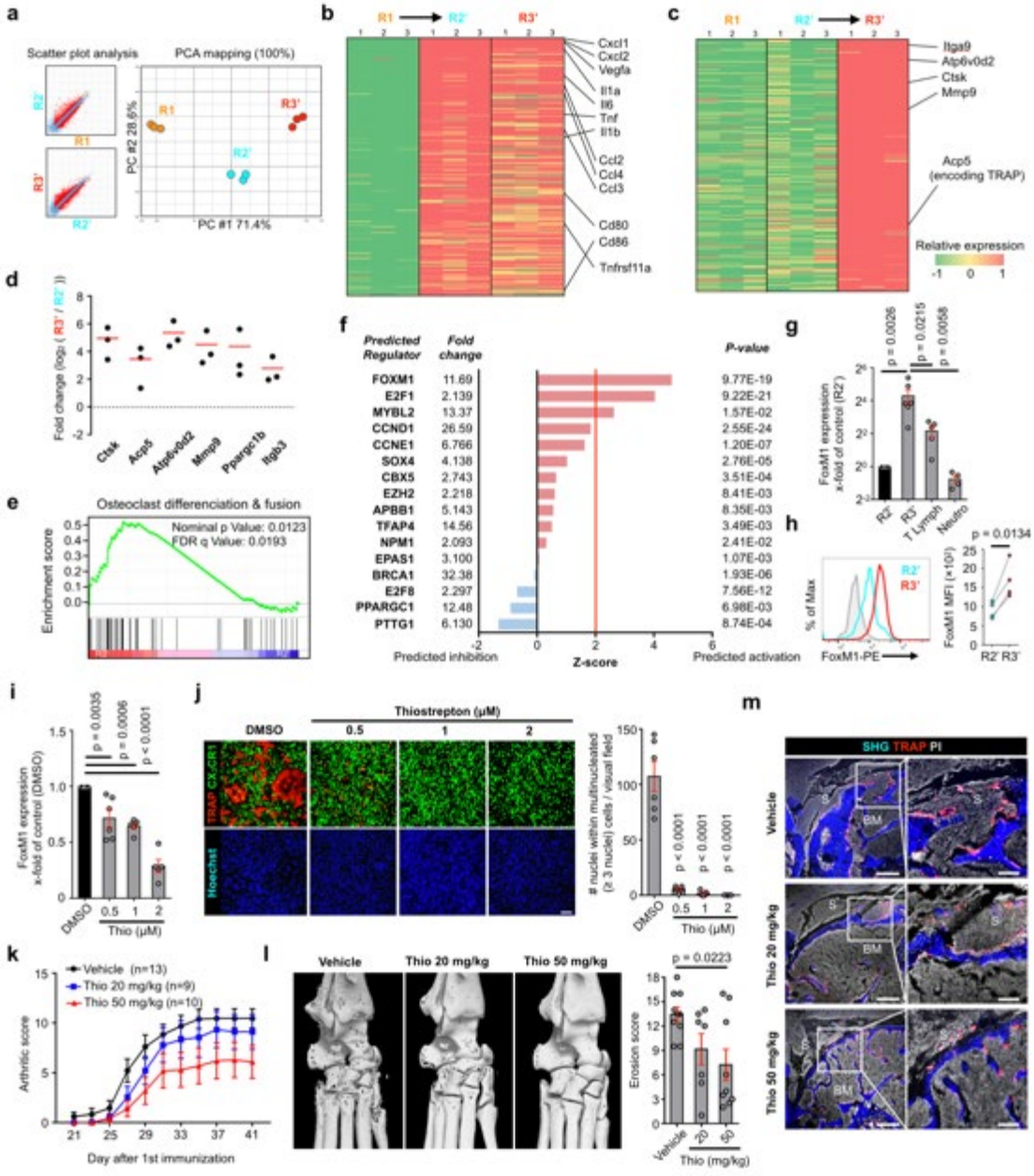

Figure 4. Transcriptional profiling by RNA-Seq identifies FoxM1 as a key regulator of R3' cells.

a, Scatter plot analysis and principal component analysis (PCA) of R1, R2', and R3' cells by RNA-Seq.

b, The top 300 upregulated genes from R1 to R2’ cells, and **c,** R2’ to R3’ cells.

d, Expression analysis of osteoclast marker genes in R3’ cells. Values indicate the fold change of FPKM in R3’/R2’ cells.

e, Enrichment analysis of osteoclast differentiation and fusion genes in R3’ cells compared to R2’ cells.

f, Upstream regulator analysis of differentially expressed genes among upregulated transcription factors in R3’.

g, RT-PCR analysis of FoxM1 expression in R2’ cells, R3’ cells, T lymphocytes, and neutrophils from the inflamed synovium.

h, Representative histogram plots and quantitative MFI of FoxM1 expression in R2’ and R3’ cells. Shaded regions indicate staining with isotype control.

i, RT-PCR analysis of FoxM1 expression in R3’ cells after incubation with thiostrepton for 48 hours.

j, Inhibition of RANKL-induced osteoclastogenesis of R3’ cells by thiostrepton. Bar, 100 μm.

k, Clinical arthritic scores of CIA mice treated with vehicle, 20 mg/kg, or 50 mg/kg thiostrepton.

l, Representative 3D reconstructions and erosion scores of rear paws by micro-CT analysis.

m, Histological examination of inflamed knee joints. Images are representative of at least three similar experiments. Bars, 300 and 100 μm.

Paired two-tailed *t* test (h) and one-way ANOVA with Bonferroni's post hoc test (g, i, j, l). Mean ± S.E.M. for each group. Symbols represent individual mice.

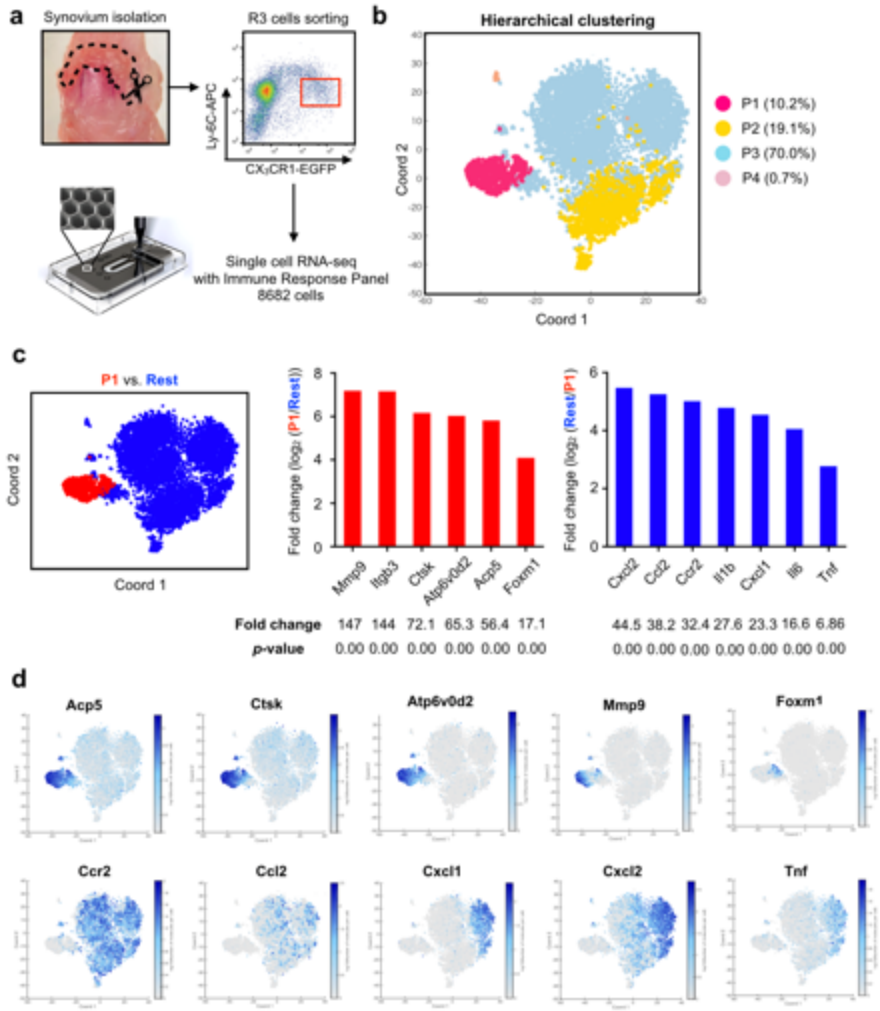

Figure 5. Single cell RNA-sequencing analysis of synovial R3 cells

a, Schematic diagram outlining the single cell RNA-sequencing analysis. R3 cells were isolated from inflamed knee synovium 1 week after CIA onset.

b, t-SNE plot of the single cell RNA-seq data of 8,682 R3 cells from CIA mice. Hierarchical clustering based on gene expression profiles was performed by BD Data View software.

c, Differential expression analysis of cluster P1 and the other cell clusters. Fold change and significance level (*p*-value) were calculated for differentially expressed genes.

d, Single gene expression plot on t-SNE plot of the single cell RNA-seq data.

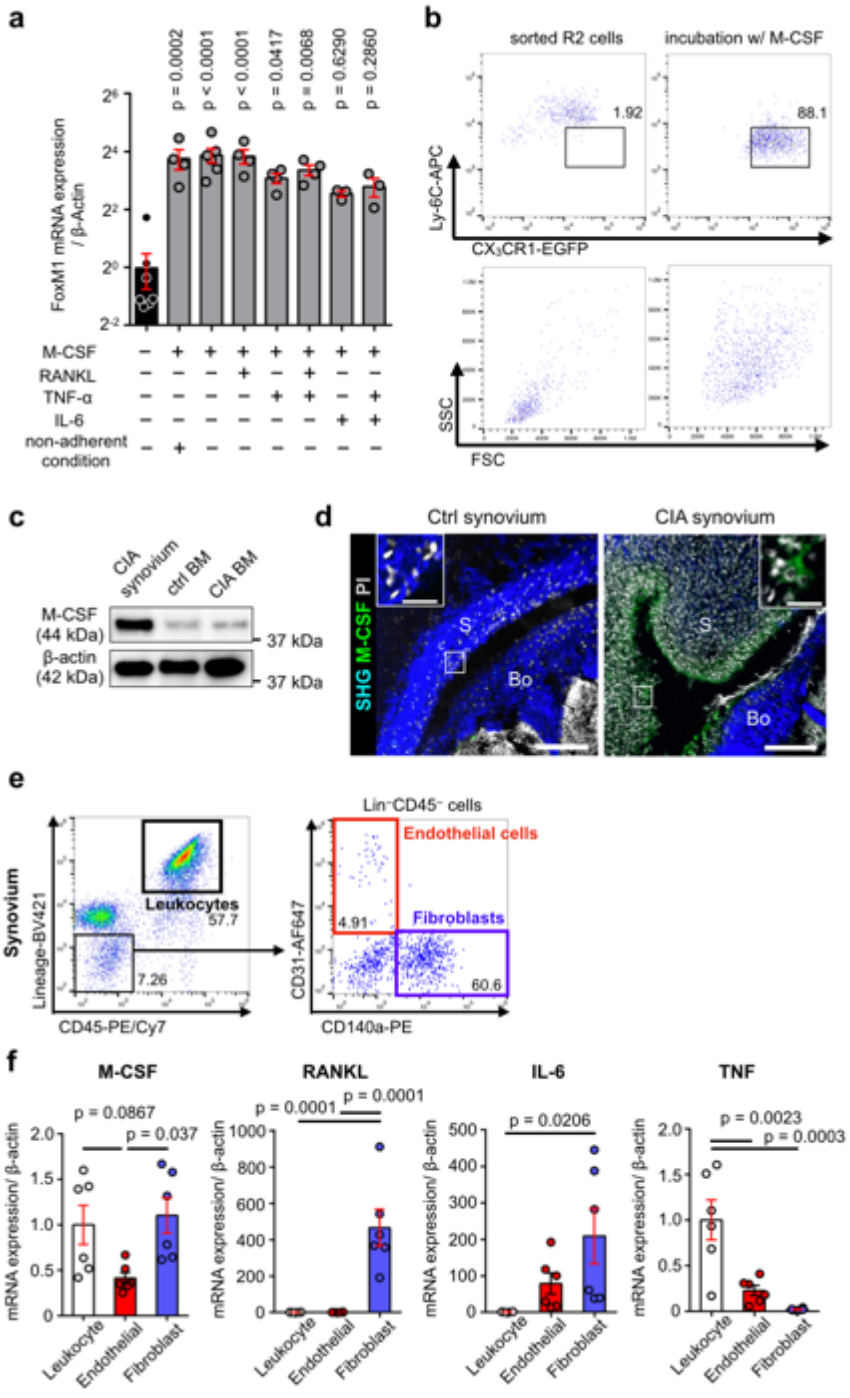

Figure 6. M-CSF mediates R2 to R3 transition and upregulates FoxM1 expression.

a, FoxM1 RT-PCR analysis in FACS-sorted R2 cells from inflamed knee joints after incubation with the indicated cytokines for 72 hours. Nunclon Sphera plates were used for non-adherent conditions. 10 ng/ml M-CSF, 100 ng/ml RANKL, 100 ng/ml TNF-α, and 100 ng/ml IL-6 were used. For the M-CSF (−) group, R2 cells were sorted and directly examined by RT-PCR analysis.

b, Representative plots of FACS-sorted R2 cells from inflamed knee joints before and after incubation with 10 ng/ml M-CSF. Similar results were obtained in three independent experiments.

c, M-CSF western blot analysis of CIA knee synovium, control bone marrow, and bone marrow from CIA mice.

d, Representative confocal images of control and CIA knee synovium stained with anti-M-CSF biotinylated antibody, followed by staining with streptavidin-FITC.

e, Gating strategy for leukocytes (Lin^+CD45^+ cells), endothelial cells ($Lin^-CD45^-CD31^+CD140a^-$ cells), and fibroblasts ($Lin^-CD45^-CD140a^+CD31^-$ cells) in the inflamed knee synovium of CIA mice.

f, M-CSF, RANKL, IL-6, and TNF RT-PCR analysis in FACS-sorted leukocytes, endothelial cells, and fibroblasts according to the protocol in **e**.

One-way ANOVA with Bonferroni's post hoc test (a, f). Mean ± S.E.M. for each group. Symbols represent individual mice.

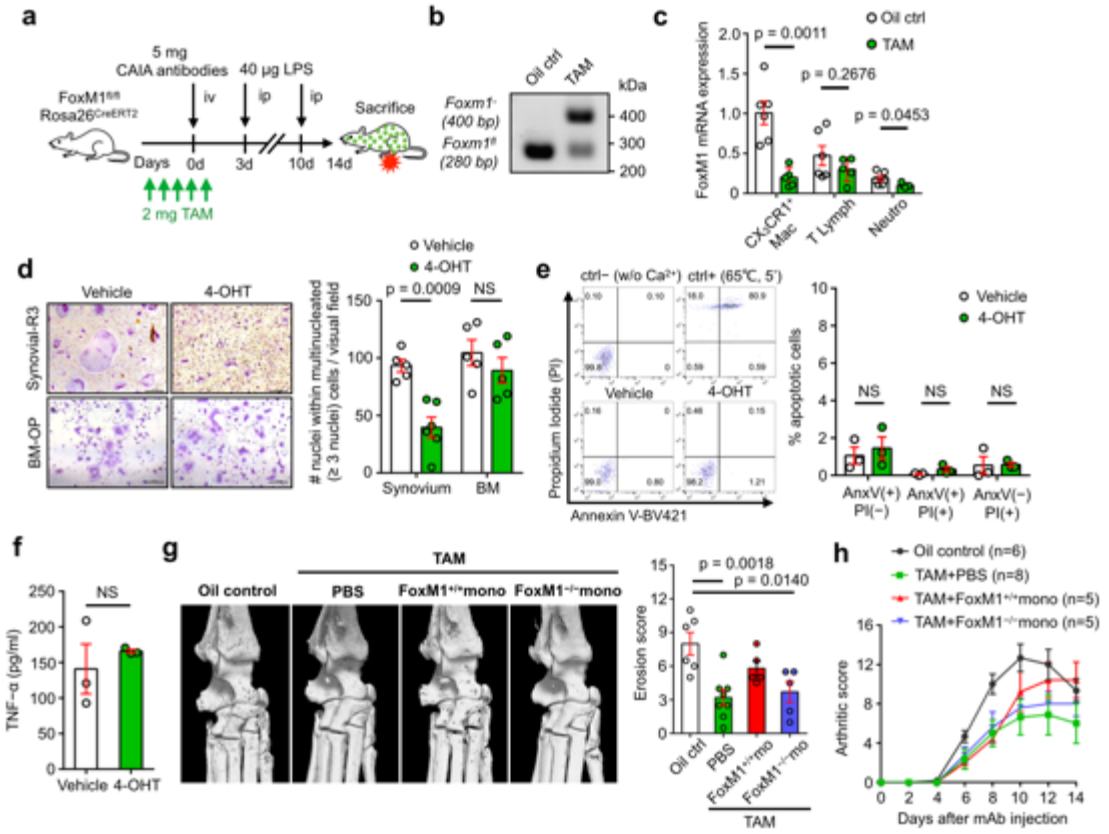

Figure 7. FoxM1 contributes to arthritis-induced bone destruction

a, Experimental design schematic for the collagen antibody-induced arthritis (CAIA) model.

b, Semi-quantitative PCR analysis to detect the deletion of FoxM1 (*FoxM1*$^{-}$) and the loxP-flanked FoxM1 allele (*FoxM1*^{fl}) in the genomic DNA of bone marrow cells.

c, FoxM1 RT-PCR analysis in CX_3CR1^+ monocytes/macrophages, $CD3^+$ T lymphocytes, and $Ly6G^+$ neutrophils in bone marrow treated with oil control or tamoxifen *in vivo*.

d, RANKL-induced osteoclastogenesis of R3 cells from inflamed knee synovium and BM-OPs from control BM with vehicle or 4 μM 4-hydroxytamoxifen (OHT). Bars, 200 μm.

e, Flow cytometry analysis of annexin-V and propidium iodide (PI) positive synovial R3 cells treated with vehicle or 4 μM 4-OHT for 72 hours.

f, Enzyme-linked immunosorbent assay (ELISA) of TNF-α in cell culture supernatant of synovial R3 cells treated with vehicle or 4 μM 4-OHT for 48 hours.

g, Representative 3D reconstructions and erosion scores of rear paws by micro CT analysis. CAIA mice treated with oil control, tamoxifen, tamoxifen plus adoptive transfer of $FoxM1^{+/+}CX_3CR1^+$ cells or $FoxM1^{-/-}CX_3CR1^+$ cells were analyzed.

h, Clinical arthritic scores of CAIA mice.

Unpaired two-tailed *t* test (c, d, e, f) and one-way ANOVA with Bonferroni's post

hoc test (g). Mean ± S.E.M. for each group. Symbols represent individual mice.

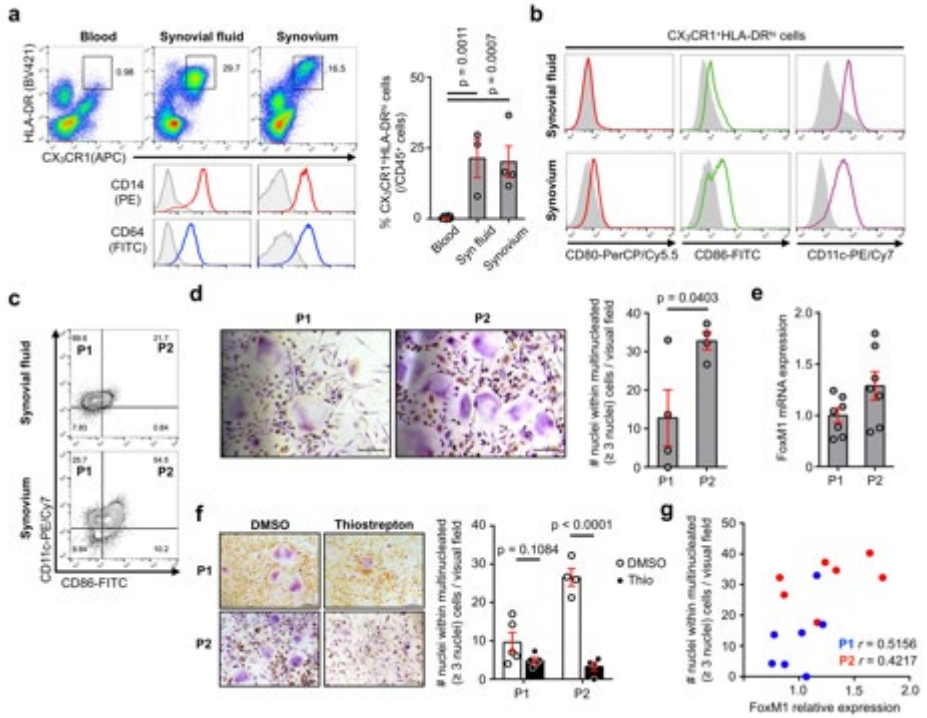

Figure 8. RA synovial $CX_3CR1^+HLA\text{-}DR^{hi}CD11c^+CD86^+$ cells have high osteoclastogenic potential

a, Phenotypic characterization of $CD45^+CX_3CR1^+HLA\text{-}DR^+$ cells in the blood, synovial fluid, and synovium of RA patients.

b, Phenotypic characterization with indicated cell surface markers on $CX_3CR1^+HLA\text{-}DR^{hi}$ cells of synovial fluid and synovium of RA patients. Shaded regions indicate staining with isotype controls.

c, Contour plots of $CD45^+CX_3CR1^+HLA\text{-}DR^{hi}$ cells gated by CD11c and CD86. $CD11c^+CD86^-$ cells were termed P1 cells and $CD11c^+CD86^+$ cells were termed P2 cells.

d, RANKL-induced osteoclastogenesis of $CX_3CR1^+HLA\text{-}DR^{hi}CD11c^+CD86^-$ cells (P1) and $CX_3CR1^+HLA\text{-}DR^{hi}CD11c^+CD86^+$ cells (P2) from synovial fluid of RA patients. Bars, 200 μm.

e, FoxM1 RT-PCR analysis in $CX_3CR1^+HLA\text{-}DR^{hi}CD11c^+CD86^-$ cells (P1) and $CX_3CR1^+HLA\text{-}DR^{hi}CD11c^+CD86^+$ cells (P2).

f, RANKL-induced osteoclastogenesis of $CX_3CR1^+HLA\text{-}DR^{hi}CD11c^+CD86^-$ cells (P1) and $CX_3CR1^+HLA\text{-}DR^{hi}CD11c^+CD86^+$ cells (P2) treated with DMSO or 0.1 μM thiostrepton. Bars, 200 μm.

g, Correlation of osteoclastogenic ability and relative FoxM1 expression in $CX_3CR1^+HLA\text{-}DR^{hi}CD11c^+CD86^-$ (P1) and $CX_3CR1^+HLA\text{-}DR^{hi}CD11c^+CD86^+$ cells (P2). *r* = correlation coefficient.

One-way ANOVA with Bonferroni's post hoc test (a) and unpaired two-tailed *t* test (d, f). Mean ± S.E.M. for each group. Symbols represent individual human

patients.

Methods

Mice.

WT DBA-1/J mice were obtained from Oriental Yeast Co. in Japan. CX_3CR1-EGFP knock-in mice[46] and TRAP promoter-tdTomato transgenic mice[47] derived from the C57BL/6 (B6) background were backcrossed >10 generations onto DBA-1/J mice. The FoxM1 LoxP/LoxP (fl/fl) mice were bred with Rosa26-CreERT2 mice by one of our co-authors, Dr. Hirao (Kanazawa University, Japan). LysM-Cre transgenic mice were provided by Dr. Shizuo Akira (Osaka University, Japan)[48]. All mice were bred and maintained under specific-pathogen-free conditions at the animal facilities of Osaka University, and all animal experiments were performed in accordance with the Osaka University Animal Experimental Guidelines using approved protocols. Mutant mice were genotyped by PCR. Following primers were used to detect FoxM1 flox allele and deleted FoxM1 allele; FoxM1 flox allele (TGGCTTCCCAGCAGTACAAATC and TGCTTACAAAAGACACACTTGGACG), deleted FoxM1 allele (TGGCTTCCCAGCAGTACAAATC and

TCTCGCTCAATTCCAAGACCAG).

Samples from RA patients.

Research involving human subjects was approved by the Institutional Review Board of Osaka University with appropriate informed consent. All RA subjects with RA fulfilled the ACR 2010 Rheumatoid Arthritis classification criteria. Clinical information, including seropositivity and medication usage, was obtained by review of electronic medical records (Supplementary Table 2). Synovial tissue specimens were obtained from RA patients undergoing joint replacement surgery or synovectomy at Osaka University Hospital. The tissue was minced and digested with 3 mg/ml type I collagenase (Worthington) in HBSS, and incubated at 37°C for 30 min, with inversion every 5 min. Disaggregated tissue elements were passed through a 70 μm cell strainer. Synovial fluid samples were obtained as excess material from RA patients with knee effusion undergoing therapeutic arthrocentesis. Blood samples were obtained from RA

patients and subjected to density centrifugation using Lymphoprep (AXS) to isolate mononuclear cells.

Induction and evaluation of collagen-induced arthritis (CIA).

Arthritis was induced in DBA-1/J mice (Oriental Yeast Co.) between 8 and 10 weeks of age as described previously[49]. Chicken type II collagen (cCII; Sigma Chemical Co.) was dissolved in 0.05 M acetic acid to a concentration of 4 mg/ml by overnight rotation at 4°C and mixed with an equal volume of Freund's complete adjuvant (2 mg/ml of *Mycobacterium tuberculosis*; Chondrex). On day 0, DBA-1/J mice were immunized at the base of the tail with 100 μl of emulsion. The same injection was repeated on day 21. The severity of arthritis was evaluated using an established semi-quantitative scoring system with a five-point scale, where 0 = no swelling, 1 = mild swelling confined to the tarsals or ankle joint, 2 = mild swelling extending from the ankle to the tarsals, 3 = moderate swelling extending from the ankle to metatarsal joints, and 4 = severe swelling encompassing the ankle, foot, and digits. The cumulative score for the

four paws of each mouse (maximum score 16) was used as the arthritis score to represent overall disease severity, as described previously[49].

Induction and evaluation of collagen antibody-induced arthritis (CAIA).

Arthritis was induced by injecting 5 mg of 5-clone Arthrogen-CAIA antibody (Chondrex) intravenously on day 0, and 40 μg of lipopolysaccharide intraperitoneally on days 3 and 10. Mice were evaluated on day 14. The severity of arthritis was evaluated with the same semi-quantitative method used for the CIA model.

For $FoxM1^{+/+}$ monocyte adoptive transfer, $CX_3CR1^{+}Ly6C^{hi}$ monocytes from the BM of WT mice were sorted using an SH800 cell sorter (Sony). For $FoxM1^{-/-}$ monocyte adoptive transfer, $CX_3CR1^{+}Ly6C^{hi}$ monocytes from the bone marrow of $FoxM1^{fl/fl}Rosa26^{CreERT2}$ mice treated with 2 mg tamoxifen for 5 days were sorted. Aliquots of 1×10^6 cells per mouse were administered intravenously to the tamoxifen-treated mice intravenously on days 1, 6, and 12.

Induction of DSS colitis.

To induce acute colitis, mice received 2% dextran sulphate sodium (DSS) salt (Wako) *ad libitum* in sterile drinking water. Mice were then sacrificed on day 6.

Parabiosis.

Male 8 week-old double transgenic mice (CX_3CR1-EGFP/TRAP-tdTomato) were surgically connected to wild-type mice as described previously[50]. The mice were anesthetized with isoflurane. The lateral aspects of each mouse were shaved and treated with hair-removal lotion (Epilat; Kracie Holdings). After corresponding lateral skin incisions were made from elbow to knee in each mouse, the forelimbs and hind limbs were tied together using silk sutures. Incisions of approximately 1 cm were made in the peritoneum of each mouse, and the mice were attached using silk sutures. The skin incisions were closed using stainless steel wound clips. To ensure the animals' wellbeing for 8 weeks, individual parabiotic mouse pairs were placed in clean cages, and food pellets were broken into pieces, soaked in water, and placed on the floor to minimize

the strain of reaching for food. Shared blood circulation was confirmed by the presence of $EGFP^+$ monocytes in the peripheral blood of wild-type parabionts.

Bone marrow transplantation.

Recipient mice were administered a single 10-Gy dose of whole-body irradiation. After 6 h, 3 million unfractionated bone marrow cells from donor mice were injected intravenously. Bone marrow reconstitution was confirmed by immunohistological analysis of tdTomato and $EGFP^+$ cells in the bone marrow at the observation endpoint.

Isolation of leukocytes from tissues.

Tissues were harvested and prepared as follows. After sacrifice under anaesthesia, the right auricles of the mice were cut and 15 ml of pre-warmed 1× PBS was injected into the left ventricle for perfusion. Perfusion was omitted in experiments designed to assess blood samples.

Because knee joints are covered with muscles, direct macroscopic observation of arthritis is challenging. Therefore, we selected mice with arthritic paws and confirmed substantial inflammation in knee joints by direct exposure of the inflamed synovium using the following protocol. Mice were perfused with 15 ml of pre-warmed 1× PBS. After the removal of the skin and biceps femoris muscle, the quadriceps femoris muscles including the vastus intermedius muscle were pinched and lifted with tweezers. The quadriceps femoris muscles and patellar ligament, including the patella, were removed from the knee joint under a stereoscopic microscope (SMZ 745T, Nikon). The hypertrophied synovium was isolated without damaging the bone (Supplementary Fig. 1b). Ankle joint tendons, including the Achilles tendon, were removed revealing the hypertrophied synovium around the talus, which allowed for isolation without damaging the bone (Supplementary Fig. 1d). Synovial tissues were digested with 3 mg/ml type I collagenase in HBSS, and incubated at 37°C for 30 min. Disaggregated tissue elements were passed through a 70 μm cell strainer.

The bone marrow, spleen, and liver were minced and passed through a 70 μm cell strainer. The kidney, lung, and brain were harvested, minced, and digested for 30 min in RPMI containing 1 mg/ml type I collagenase (Worthington) and 5% heat-inactivated foetal bovine serum (FBS) at 37°C to obtain single-cell suspensions. For isolation of colonic lamina propria cells, the entire colon was cut longitudinally and washed to remove all excess fat and faeces. The tissues were then incubated in calcium/magnesium-free Hank's Balanced Salt Solution (HBSS) containing 5 mM EDTA at 37°C for 20 min on a shaking incubator. After removal of epithelial cells, the tissues were finely minced and incubated in RPMI containing 1 mg/ml type IV collagenase, 600 U/ml DNase IV (Qiagen), 0.5 mg/ml of Dispase (Invitrogen), and 5% FBS for 50 min at 37°C in a shaking incubator. The resulting cell suspension was passed through a 70 μm cell strainer, and centrifuged at 1500 rpm for 5 min to prepare for FACS analysis.

Flow cytometry.

Measurements were performed on an SH800 cell sorter (Sony) and analyzed with FlowJo software (TreeStar). Isolated murine cells were blocked with anti-CD16/32 antibody (553141; BD Biosciences) for 10 min, followed by staining with the following antibodies for 15 min: anti-CD45-PB (103126; BioLegend), anti-CD80-PB (104724; BioLegend), anti-CD86-PB (105021; BioLegend), anti-CD3-BV421 (100227; BioLegend), anti-Ly6G-BV421 (127627; BioLegend), Streptavidin-BV421 (405226; BioLegend), anti-F4/80-BV421 (123137; BioLegend), anti-CD11b-BV421 (101235; BioLegend), anti-I-A/I-E-Biotin (107603; BioLegend), anti-CD11c-Biotin (117303; BioLegend), anti-CD265 (RANK)-Biotin (13-6612-81; eBioscience), Lineage cell detection cocktail-Biotin (130-092-613; Miltenyi Biotec), anti-CD3-PE (100308; BioLegend), anti-CD140a-PE (135905; BioLegend), anti-CD45-FITC (103108; BioLegend), anti-CX_3CR1-FITC (149019; BioLegend), anti-Ly6C-APC (560595; BD Biosciences), anti-CX_3CR1-APC (149007; BioLegend), Annexin V-APC (640919; BioLegend), anti-CD45-PE/Cy7 (103114; BioLegend), anti-CD31-AF647 (102516; BioLegend), anti-CD11b-PE/Cy7 (552850; BD

Biosciences), anti-F4/80-PE/Cy7 (123113; BioLegend), anti-CCR2-PE/Cy7 (150611; BioLegend), Biotin-Rat IgG2a,κ isotype control (400503; BioLegend), PB-Rat IgG2a,κ isotype control (400527; BioLegend), PB-Armenian Hamster IgG isotype control (400925; BioLegend), BV421-Rat IgG2a, κ isotype control (BD Biosciences), and PE/Cy7-Rat IgG2a, κ isotype control (400521; BioLegend). Annexin V-BV421 (640923; BioLegend) and Propidium iodide (PI) solution (421301; BioLegend) were used to evaluate apoptosis.

The following antibodies were used for human samples: anti-HLA-DR-BV421 (307635; BioLegend), anti-CD64-FITC (305005; BioLegend), anti-CD86-FITC (374203; BioLegend), anti-CD14-PE (325605; BioLegend), anti-CX_3CR1-APC (341609; BioLegend), anti-CD80-PerCP/Cy5.5 (305231; BioLegend), anti-CD45-PE/Cy7 (304015; BioLegend), anti-CD11c-PE/Cy7 (561356; BD Biosciences), PE-mouse IgG1κ isotype control (400111; BioLegend), FITC-mouse IgG1κ isotype control (400107; BioLegend), PerCP/Cy5.5-mouse IgG1κ isotype control (400149; BioLegend), and Fc blocker (422301; BioLegend).

For intracellular FoxM1 staining, 200 µl of fixation/permeabilization working solution (00-5523-00; eBioscience) was added to each sample, and incubated for 60 min at room temperature. After blockade with anti-CD16/32 antibody, FoxM1 antibody (175798; Abcam) in 100 µl of permeabilization buffer (00-5523-00; eBioscience) was added to each sample. Samples were subsequently incubated for 60 min at room temperature, and then washed with 200 µl of permeabilization buffer. Anti-rabbit biotinylated antibody (BA-1000; Vector) was added in 50 µl of permeabilization buffer and samples were incubated for 30 minutes at room temperature, washed with 200 µl of permeabilization buffer, and then stained with Streptavidin-PE (405203; BioLegend) or Streptavidin-BV421 (405226; BioLegend) for 30 min at room temperature. Normal rabbit IgG (sc-2027; Santa Cruz Biotechnology) was used as a control antibody.

Histology and immunohistochemistry.

Mice were euthanized at various time points and tissues were fixed by perfusion with 4% paraformaldehyde (PFA). Dissected knee joints were further fixed with 4% PFA for 3 h at 4°C. The samples were frozen in chilled hexane (Wako) using dry ice, and 12-μm-thick sections of non-decalcified knee joints were prepared using a Multi-Purpose Cryosection Preparation Kit[51] (Section-Lab and Leica Microsystems). A standard protocol was used for haematoxylin and eosin (H&E) staining, and immunohistological analyses were performed as described previously[14]. Fluorescence-based staining for tartrate-resistant acid phosphate (TRAP) with ELF97 substrate (Life Technologies) was used with some modifications. Anti-M-CSF antibody (sc-365779; Santa Cruz Biotechnology) was biotinylated in our laboratory using a Biotin Labelling Kit-NH_2 (Dojindo Molecular Technologies Inc.). Samples were stained with anti-M-CSF biotinylated antibody in TBS-T for 60 min at room temperature, followed by staining with Streptavidin-FITC (405201; BioLegend) for 60 minutes at room temperature. Samples were observed using a TCS-SP5 confocal microscope (Leica Microsystems) and illuminated with a laser (wavelength: 405 nm for ELF97 and

BV421, 488 nm for EGFP, and 561 nm for PI and tdTomato). Collagen-enriched bone matrices and synovial fibrous tissues were visualized using the second harmonic generation (SHG) with infrared lasers of a TCS-SP5 multi-photon laser microscope (wavelength 880 nm) driven by a Chameleon XR Sapphire laser (Coherent), which also excite EGFP. Emission signals were obtained by setting the wavelength to 420–470 nm for BV421, 500–550 nm for ELF97, EGFP, and FITC, 580–630 nm for tdTomato, 600–630 nm for PI, and 430–480 nm for SHG. For cell counting of healthy synovium, synovial fibres and bones were identified with SHG, and three knee joint sections per mouse were analyzed using Imaris software (Bitplane) (Supplementary Fig. 2a). Knee joints were used for histological examination because articular anatomical structures, such as synovium and bare area, were easily discerned microscopically in both inflamed and uninflamed conditions, unlike paws, where small tarsal bones tightly adhere to each other.

Real-Time PCR Analyses.

Total RNA and cDNA of the cells from each tissue were obtained with an RNeasy Mini Kit (Qiagen) and Superscript III reverse transcriptase (Thermo Fisher Scientific), according to the manufacturers' instructions. Quantitative real-time (RT) PCR was performed for 40 cycles using a Thermal Cycler Dice Real-Time System TP800 (Takara). The reactions were normalized relative to the housekeeping gene β-Actin, and the specificity of the amplified products was confirmed by dissociation curves. The following specific primer pairs were used (forward and reverse, respectively): mouse β-actin (5′-TCCTCCCTGGAGAAGAGCTA-3′ and 5′-ATCTCCTTCTGCATCCTGTC-3′); mouse FoxM1 (5′-GTCTCCTTCTGGACCATTCACC-3′ and 5′-GCTCAGGATTGGGTCGTTTCTG-3′); mouse M-csf (5'-CCCATATTGCGACACCGAA-3' and 5'-AAGCAGTAACTGAGCAACGGG-3'); mouse Rankl (5'-CAGCATCGCTCTGTTCCTGTA-3' and 5'-CTGCGTTTTCATGGAGTCTCA-3'); mouse Tnf (5'-GCCACCACGCTCTTCTGTCTAC-3' and

5’-GGGTCTGGGCCATAGAACTGAT-3’); mouse Il−6 (5’-CACATGTTCTCTGGGAAATCG-3’ and 5’-TTGTATCTCTGGAAGTTTCAGATTGTT-3’), mouse Il−1β (5’-CTGCAGCTGGAGAGTGTGGAT-3’ and 5’-CTCCACTTTGCTCTTGACTTCTATCTT-3’).

RNA-Seq.

R1, R2’, and R3’ cells from three mice were isolated using an SH800 cell sorter (Sony) and total RNA was extracted using QIAzol lysis reagent (Qiagen), according to the manufacturer’s instructions. Sequencing was performed on an Illumina HiSeq 2500 platform in 75-base single-end mode with Illumina Casava 1.8.2 software used for base-calling. Sequenced reads were mapped to the mouse reference genome sequences (mm10) using TopHat v2.0.13 in combination with Bowtie2 ver. 2.2.3 and SAMtools ver. 0.1.19. Fragments per kilobase of exon per million mapped fragments (FPKM) were calculated using Cuffkinks version 2.2.1. The Subio Platform and Subio Basic Plug-in (v1.20;

Subio Inc., Aichi, Japan) were used to calculate the between-sample fold change analyzed by two-tailed Student's t-test ($p < 0.1$). Bioinformatics analyses were performed with Ingenuity Pathway Analysis software (Ingenuity Systems; Qiagen). The FPKM score was calculated based on the number of transcribed fragments, and functional associations were computed using the Gene Set Enrichment Analysis (GSEA) software (Broad Institute; http://software.broadinstitute.org/gsea/index.jsp). Gene sets from the Broad Institute Molecular Signatures Database and a modified gene set (Supplementary Table 1) were used.

Upstream Regulator Analysis in QIAGEN's Ingenuity Pathway Analysis (IPA; Qiagen) was performed to predict the activation or inhibition of transcription factors based on the observed gene expression changes in the gene datasets and the direction of expression changes in R2' vs. R3' cells. Statistical analysis of the predictions was calculated by the activation z score, ''which is designed such that gene sets composed of randomly chosen perturbed genes with random sign of fold change do not lead to significant results on average''

(Ingenuity Downstream Effects Analysis, whitepaper). The strongest predicted activation corresponds to z-scores ≥ 2, and the strongest predicted inhibition corresponds to z-scores ≤ −2.

Single cell RNA-sequencing analysis

R3 cells were isolated from the inflamed knee synovium of CIA mice 1 week after arthritis onset. Then, targeted single-cell RNA-sequence analysis was conducted using the BD Rhapsody Single-Cell Analysis System (BD BioScience), following the manufacture's protocol. In short, the single cell suspension was loaded into a BD Rhapsody cartridge with >200,000 microwells and single cell capture was achieved by random distribution and gravity precipitation. Next, the bead library was loaded into the microwell cartridge to saturation, to promote the pairing of each cell with a bead. The cells were lysed in the microwell cartridge to hybridize mRNA molecules to barcoded capture oligos on the beads. Then, beads were collected from the microwell cartridge into a single tube for subsequent cDNA synthesis, ExoI digestion and

multiplex-PCR based library construction. For the library construction, we used the customized BD Rhapsody Immune Response Panel for mouse (BD BioScience) consisting of primer sets for 404 genes. Sequencing was performed on an Illumina HiSeq 3000 platform. The BD Rhapsody Analysis Pipeline was used to process the sequencing data (fastq files) and output result files were analyzed and visualized by the BD Data view software (BD BioScience). Raw reads from these samples were submitted to the National Center for Biotechnology Information (NCBI) Gene Expression Omnibus database (accession no. GSM3712154).

Micro-computed tomography (micro-CT) of bone tissues.

With regard to bone erosion, arthritic hind limbs were scanned with micro-CT (ScanXmate-RX; Comscantechno Inc.), and 3D microstructure images were generated using TRI/3D-BON software (RATOC Systems). The severity of periarticular erosions was determined by two blinded observers (TH and JK) using a semi-quantitative method with modifications from a previous report[19]. Six

sites in the ankle joint were scored: the talus; the navicular bone; the medial cuneiform bone; and the bases of the first, second, and third metatarsals (Supplementary Fig. 9a). Each site was scored on a scale of 0–3 (0 = normal, 1 = pitting, 2 = full-thickness holes in small–medium areas, 3= full-thickness holes in medium–large areas) with a maximum score of 18 as described in Supplementary Fig 9b. The scores of the arthritic hind paw determined by the two observers were averaged to obtain the final erosion score. Inter-observer and intra-observer reproducibility are shown in Supplementary Fig. 9c, d. We used ankles for micro CT analysis because official radiographic quantification of bone erosion in human RA patients is done in wrists or ankles (Sharp score).

Trabecular bone morphometry within the metaphyseal region of the distal femur was quantified using micro-CT. 3D microstructure images were generated and bone analysis was performed using TRI/3D-BON software (RATOC Systems), as described previously.[52]

Western blotting analysis.

Whole-cell protein extracts of inflamed synovium and bone marrow were prepared using radioimmunoprecipitation assay (RIPA) buffer (1× PBS, 0.1% sodium dodecyl sulphate (SDS), 1% NP40, 0.5% sodium deoxycholate) supplemented with protease inhibitors (Sigma), and centrifuged at 4°C for 10 min at 14000 × *g*. Protein concentration was determined by BCA protein assay (Thermo Scientific). Equal amounts of protein were subjected to electrophoresis on 4%–15% gradient SDS-polyacrylamide gels (Bio-Rad) and transferred to PVDF membranes. After blocking with PVDF blocking reagent (Toyobo), the membranes were incubated with primary antibodies in Immunoreaction Enhancer Solution 1 (Toyobo) for 1 h at room temperature followed by incubation with secondary antibody in Immunoreaction Enhancer Solution 2 (Toyobo) for 1 h at room temperature. The following antibodies were used at the indicated dilutions: β-actin (20272; Abcam; 1:1000), M-CSF (1:1000).

Analysis of TNF−α in cell culture supernatants

CAIA was induced in FoxM1$^{fl/fl}$Rosa26^{CreERT2} mice and 1 × 10^4 R3 cells from inflamed synovium of knee and ankle joints were sorted using SH800 (Sony). After 48 h of incubation with EtOH or 4 μM 4-hydroxytamoxifen (4-OHT), culture medium was replaced and incubated for 24 h with 10 ng/ml M-CSF in minimal essential medium (MEM). The TNF−α concentration in cell culture supernatant was determined with the enzyme linked immunosorbent assay (ELISA), using the Mouse TNF alpha ELISA Kit (ab100747; Abcam), based on the manufacturer's protocol.

Treatment with thiostrepton *in vivo.*

CIA mice were divided into three treatment groups: vehicle (20% *N*,*N*-dimethylacetamide, 75% polyethylene glycol 400, and 5% Tween 80), low-dose thiostrepton, and high-dose thiostrepton. Thiostrepton was injected intraperitoneally at a dose of 20 mg/kg (low-dose) or 50 mg/kg (high-dose) every other day for 3 weeks before sacrifice. For RT-PCR analyses of the inflamed

synovium, CIA mice were sacrificed 2 weeks after starting treatment with vehicle or 50 mg/kg thiostrepton injection every other day.

For the physiological bone remodelling analyses, male mice were divided into two groups: vehicle (20% *N*,*N*-dimethylacetamide, 75% polyethylene glycol 400, and 5% Tween 80), and 50 mg/kg thiostrepton. Vehicle or thiostrepton was injected intraperitoneally twice a week from 5 weeks of age, and mice were sacrificed at 10 weeks of age.

***In vitro* osteoclast differentiation.**

For murine samples, FACS-sorted primary blood monocytes and synovial monocytes/macrophages (1×10^4 cells per samples) were cultured with 10 ng/ml M-CSF in MEM containing 10% FCS. After 2 days, cells were cultured for 3 days in MEM containing 10 ng/ml M-CSF and 100 ng/ml RANKL unless otherwise noted. Murine TNF−α (315-01A; PeproTech), murine IL−6 (406-ML; R&D systems), and murine osteoprotegerin (459-MO; R&D systems) were added at the concentrations indicated in the figure legends. Nunclon Sphera plates

(174927; Thermo Fisher Scientific) were used for non-adherent conditions. Bone marrow OP-containing populations (BM-OPs) represent the $CD45^{+}CX_3CR1^{+}Ly6C^{hi}$ bone marrow population with osteoclast precursor activity[8,13].

For human samples, FACS-sorted cells (2×10^4 cells per samples) were cultured with 30 ng/ml M-CSF in MEM containing 10% FCS for 2 days, followed by incubation with 30 ng/ml M-CSF and 100 ng/ml RANKL for 9 days.

Sorting of mature osteoclasts from RepCell

To avoid cell damage during isolation of osteoclasts from plates, the temperature-responsive cell cultureware, RepCell (CellSeed), was used. Multiple CIA mice (CX_3CR1-EGFP/TRAP-tdTomato) were sacrificed to isolate 1×10^5 R3 cells from inflamed knee and ankle joints. Sorted R3 cells were incubated with 10 ng/ml M-CSF for 48 h, followed by incubation with 10 ng/ml M-CSF and 100 ng/ml RANKL for 96 h to induce osteoclastogenesis. Cells were gently collected after a 10 min incubation at 4°C and stained with Hoechst 33342

(1:1000). The multinucleated $FSC^{hi}SSC^{hi}tdTomato^{+}$ cell population were gated and sorted by flow cytometry.

Bone resorption assay.

Primary blood monocytes, synovial macrophages, and BM-OPs were isolated from CIA mice, sorted onto Osteo Assay Surface plates (Corning) coated with inorganic crystalline calcium phosphate, and cultured with 100 ng/ml RANKL and 10 ng/ml M-CSF for 6 days. After removing cells with sodium hypochlorite, resorption pits were photographed and analyzed using a BZ-X700 fluorescence microscope (Keyence).

Electroporation

Bone marrow-derived macrophages were obtained from WT mice by culturing bone marrow cells collected from the tibias and femurs of 8–10-week-old males. Pelleted cells (1×10^6 cells per sample) were suspended in 100 µl of Mouse Macrophage Nucleofector Solution (Lonza, VPA-1009) and we combined the

cell suspension with cytomegalovirus promoter (CMV)-T7-tagged FoxM1 plasmid (CMV-T7-FoxM1; a gift from Dr. Pradip Raychaudhuri) or mock plasmid. The cell/DNA suspension was transferred into an Amaxa electrode cuvette and electroporated in Amaxa Nucleofector Device Ⅱ using program Y-001. Then, the cells were cultured in MEM supplemented with 10 ng/ml M-CSF for 48 hours for real-time PCR analyses. To analyze osteoclast differentiation, cells were cultured for an additional 4 days in MEM containing 100 ng/ml RANKL and M-CSF at the indicated concentrations.

Statistical Analysis.

The results are shown as single data points in a scatter dot plot and as mean ± SEM. Between group differences were determined using the two-tailed *t* test. One-way ANOVA with Bonferroni's post hoc test was used for comparisons among three or more groups. Associations were assessed using Pearson's correlation. Statistical analyses were performed using GraphPad Prism

(GraphPad Software). Statistical methods to predetermine sample size were not applied. Animal and human sample sizes are indicated on scatter dot plots.

Data availability.

The data sets analyzed during the current study are available from the corresponding author upon reasonable request. Access to raw RNA-seq data related to this study is available through the Gene Expression Omnibus (GEO) (accession number: GSE 117149 and GSM 3712154 for single cell RNA-seq).

46. Jung, S. *et al.* Analysis of fractalkine receptor CX3CR1 function by targeted deletion and green fluorescent protein reporter gene insertion. *Mol. Cell. Biol.* **20**, 4106–4114 (2000).

47. Kikuta, J. *et al.* Dynamic visualization of RANKL and Th17-mediated osteoclast function. *J. Clin. Invest.* **123**, 866–873 (2013).

48. Takeda, K. *et al.* Enhanced Th1 activity and development of chronic

enterocolitis in mice devoid of Stat3 in macrophages and neutrophils. *Immunity* **10**, 39–49 (1999).

49. Brand, D. D., Latham, K. A. & Rosloniec, E. F. Collagen-induced arthritis. *Nat. Protoc.* **2**, 1269–1275 (2007).

50. Kamran, P. *et al.* Parabiosis in mice: a detailed protocol. *J. Vis. Exp.* 1–5 (2013). doi:10.3791/50556

51. Kawamoto, T. Use of a new adhesive film for the preparation of multi-purpose fresh-frozen sections from hard tissues, whole-animals, insects and plants. *Archives of Histology and Cytology* **66**, 123–143 (2003).

52. Ishii, M., Kikuta, J., Shimazu, Y., Meier-Schellersheim, M. & Germain, R. N. Chemorepulsion by blood S1P regulates osteoclast precursor mobilization and bone remodeling in vivo. *J. Exp. Med.* **207**, 2793–2798 (2010).